The designer cytokine IC7Fc attenuates atherosclerosis development by targeting hyperlipidemia in mice

Panhuis, W.I.H.; Thiemann, E.; Dijk, D.M.A.H. van; Been, B.; Jarrett, K.E.; Meurs, A.; ... ; Schönke, M.

Citation
Panhuis, W. I. H., Thiemann, E., Dijk, D. M. A. H. van, Been, B., Jarrett, K. E., Meurs, A., … Schönke, M. (2025). The designer cytokine IC7Fc attenuates atherosclerosis development by targeting hyperlipidemia in mice. *Science Advances*, *11*(43). doi:10.1126/sciadv.adx3794

Version:	Publisher's Version
License:	Creative Commons CC BY-NC 4.0 license
Downloaded from:	https://hdl.handle.net/1887/4295830

Note: To cite this publication please use the final published version (if applicable).

Check for updates

MOLECULAR BIOLOGY

The designer cytokine IC7Fc attenuates atherosclerosis development by targeting hyperlipidemia in mice

Wietse In het Panhuis[1,2,3,4], Ellen Thiemann[1,2], Daisy M. A. H. van Dijk[1,2], Bibian Been[1,2], Kelsey E. Jarrett[5], Amber Meurs[6], Sander Kooijman[1,2], Milaine V. Hovingh[7], Melanie Modder[1,2], Bram W. van Os[8,9,10], Thijs J. Sluiter[2,11], Niek Blomberg[12], Amanda C. M. Pronk[1,2], Salwa Afkir[1,2], Trea C. M. Streefland[1,2], Reshma A. Lalai[1,2], Maria O. Taveras[13], Sen Zhang[1,2], Timothy E. Adams[14], Lauren V. Terry[15], Sarah M. Turpin-Nolan[15], Margreet R. de Vries[2,11,16], Martin Giera[12], Stefan Rose-John[17], Noam Zelcer[6], Jan Freark de Boer[7,18], Thomas Q. de Aguiar Vallim[5,13], Mark A. Febbraio[15], Patrick C. N. Rensen[1,2], Milena Schönke[1,2]*

Copyright © 2025 The Authors, some rights reserved; exclusive licensee American Association for the Advancement of Science. No claim to original U.S. Government Works. Distributed under a Creative Commons Attribution NonCommercial License 4.0 (CC BY-NC).

The chimeric cytokine IC7Fc conveys the metabolic signaling properties of the glycoprotein 130 receptor cytokines interleukin-6 and ciliary neurotrophic factor via membrane-bound signaling. IC7Fc was previously shown to slow the progression of type 2 diabetes mellitus, and here, we demonstrate its effect on atherosclerotic development. In APOE*3-Leiden.CETP mice, an atherosclerosis-prone model with a humanized lipoprotein metabolism, IC7Fc markedly lowered plasma triglyceride and total cholesterol levels. This was mechanistically explained by an inhibition of de novo lipogenesis in the liver, increased synthesis of bile acids from cholesterol, and downregulated apolipoprotein B synthesis, which resulted in decreased cholesterol secretion in very low–density lipoprotein particles. As a consequence, IC7Fc treatment considerably reduced atherosclerotic lesion formation and vascular inflammation compared with current antihyperlipidemic therapy. In conclusion, IC7Fc is a promising pharmacological treatment for cardiometabolic diseases targeting hyperlipidemia and inflammation.

INTRODUCTION

Cardiovascular diseases (CVDs), with atherosclerosis as the main underlying pathology, cause approximately 30% of deaths worldwide (*1*). Despite the use of widely prescribed drugs that target traditional risk factors, such as elevated blood pressure and high levels of low-density lipoprotein cholesterol, a substantial residual CVD risk remains (*2*). The focus is, therefore, shifting toward therapeutically targeting nontraditional risk factors including triglyceride (TG)–rich lipoproteins and inflammation (*2*–*4*). Interleukin-6 (IL-6) is one of the major cytokines released in response to infection and inflammation, and its production by myeloid cells is amplified by up to six orders of magnitude by tumor necrosis factor–α (TNF-α) (*5*). Epidemiological studies indicate that high circulating levels of IL-6 are associated with future cardiovascular risk (*6*) and the IL-6 receptor (IL-6R) locus has been positively associated with coronary artery disease in genome-wide association studies (*7*–*10*). This relationship appears to be causal as IL-6 knockout mice are protected from atherosclerosis development (*6*). Accordingly, a monoclonal antibody that inhibits IL-6 called ziltivekimab reduced atherosclerosis-related biomarkers of inflammation and thrombosis in a phase 2 clinical trial and is entering a large-scale cardiovascular outcomes trial (NCT05021835) (*11*). However, inhibition of IL-6 has also been related to increased risk of bacterial and fungal infections, and IL-6 knockout mice become obese later in life and have impaired hepatic regeneration (*5*).

This dual nature of IL-6 has been attributed to two different signaling modalities, referred to as classical signaling and trans-signaling. In the classical signaling pathway, IL-6 binds to the membrane-bound IL-6R that is present on a select range of cell types, namely, hepatocytes and certain leukocytes, resulting in the trimerization with two units of the ubiquitously expressed signal-transducing coreceptor glycoprotein 130 (gp130) (*12*). The activation of this pathway, for instance, through high circulating IL-6 levels following exercise, was shown to attenuate obesity, insulin resistance, and inflammation (*13*). In contrast, under inflammatory circumstances, the IL-6R undergoes proteolytic shedding at the membrane to form the soluble IL-6R (sIL-6R). IL-6/sIL-6R complexes can initiate gp130 homodimerization on all cells of the body, also those that do not express the IL-6R. This process, referred to as IL-6 trans-signaling, causes systemic inflammation (*14*, *15*). Moreover, blocking IL-6 trans-signaling with a soluble form of the gp130 receptor (sgp130Fc) prevents inflammation in both adipose tissue (*14*) and liver (*16*). The clinical form of sgp130Fc, termed olamkicept, was found to be both safe and effective

[1]Division of Endocrinology, Department of Medicine, Leiden University Medical Center, Leiden, Netherlands. [2]Einthoven Laboratory for Experimental Vascular Medicine, Leiden University Medical Center, Leiden, Netherlands. [3]Tytgat Institute for Liver and Intestinal Research, Amsterdam University Medical Centers, University of Amsterdam, Amsterdam, Netherlands. [4]Amsterdam Gastroenterology Endocrinology Metabolism, Amsterdam University Medical Centers, Amsterdam, Netherlands. [5]Division of Cardiology, Department of Medicine, University of California, Los Angeles, Los Angeles, CA, USA. [6]Department of Medical Biochemistry, Amsterdam UMC, Amsterdam Gastroenterology Endocrinology Metabolism and Amsterdam Cardiovascular Sciences, University of Amsterdam, Amsterdam, Netherlands. [7]Department of Pediatrics, University of Groningen, University Medical Center Groningen, Groningen, Netherlands. [8]Department of Medical Biochemistry, Amsterdam University Medical Centers, Amsterdam, Netherlands. [9]Amsterdam Cardiovascular Sciences, Atherosclerosis & Ischemic Syndromes, Amsterdam, Netherlands. [10]Amsterdam Immunity and Infection, Amsterdam, Netherlands. [11]Department of Surgery, Leiden University Medical Center, Leiden, Netherlands. [12]Center for Proteomics and Metabolomics, Leiden University Medical Center, Leiden, Netherlands. [13]Department of Biological Chemistry, University of California, Los Angeles, Los Angeles, CA, USA. [14]CSIRO Manufacturing, Clayton, Victoria, Australia. [15]Drug Discovery Biology, Monash Institute of Pharmaceutical Sciences, Monash University, Parkville, Victoria, Australia. [16]Department of Surgery, Brigham and Women's Hospital, Harvard Medical School, Boston, MA, USA. [17]Department of Biochemistry, Christian-Albrechts-Universität zu Kiel, Kiel, Germany. [18]Department of Laboratory Medicine, University of Groningen, University Medical Center Groningen, Groningen, Netherlands.
*Corresponding author. Email: m.schoenke@lumc.nl

Downloaded from https://www.science.org at Leiden University on March 06, 2026

in a phase 2 clinical trial for the treatment of inflammatory bowel disease (*17*).

To exploit the benefits of the classical IL-6 signaling while circumventing IL-6 trans-signaling, Kallen *et al.* (*18*) developed the chimeric cytokine IC7 by exchanging one of the gp130 binding sites of IL-6 for the leukemia inhibitory factor receptor (LIFR) binding module from a structurally related cytokine, ciliary neurotrophic factor (CNTF). CNTF, which also has antiobesogenic and antidiabetic effects (*19*), induces heterotrimerization of gp130 and LIFR by binding to the CNTF receptor or IL-6R, but does not induce gp130 homodimerization. Because CNTF acts mainly in the central nervous system, however, the peripheral administration of a human recombinant form of CNTF, Axokine, in humans led to the formation of anti-CNTF antibodies outside of the central nervous system, rendering it an ineffective treatment strategy (*20*). In contrast, IC7 combines IL-6–like characteristics with CNTF-binding properties, avoiding both a neutralizing antibody response and activation of the IL-6 trans-signaling pathway via gp130 homodimerization (Fig. 1A). Consequently, IC7 differs from IL-6 as it induces the heterotrimerization of LIFR (membrane bound or soluble), IL-6R, and gp130, forming a receptor complex that is not engaged by any endogenous cytokine but that is required for IC7 signaling in cells coexpressing these three receptors (*21*, *22*). To improve pharmacokinetics, IC7 was fused to the human crystallizable fragment domain (Fc) of immunoglobulin G (IgG), resulting in IC7Fc. IC7Fc treatment improved glucose tolerance and hyperglycemia and prevented weight gain and liver steatosis in obese mice, while administration to human cells in vitro and nonhuman primates resulted in no signs of inflammation or immunogenicity (*22*). The effect of IC7Fc treatment on cardiovascular health is unknown.

In this study, we aimed to assess whether targeting the IL-6 signaling pathway with the obesity and type 2 diabetes mellitus (T2DM) drug IC7Fc reduces the development of atherosclerosis in APOE*3-Leiden.CETP mice, a well-established atherosclerosis model that has a humanized lipoprotein metabolism (*23*, *24*). In these mice, IC7Fc treatment resulted in a pronounced reduction in atherosclerosis development that was caused by attenuated hyperlipidemia through reduced hepatic de novo lipogenesis and very low–density lipoprotein (VLDL) production as well as increased bile acid production in the liver.

RESULTS

IC7Fc treatment attenuates atherosclerosis progression and improves lesion stability index

To assess the efficacy of IC7Fc treatment on atherosclerosis development, we used hyperlipidemic female APOE*3-Leiden.CETP

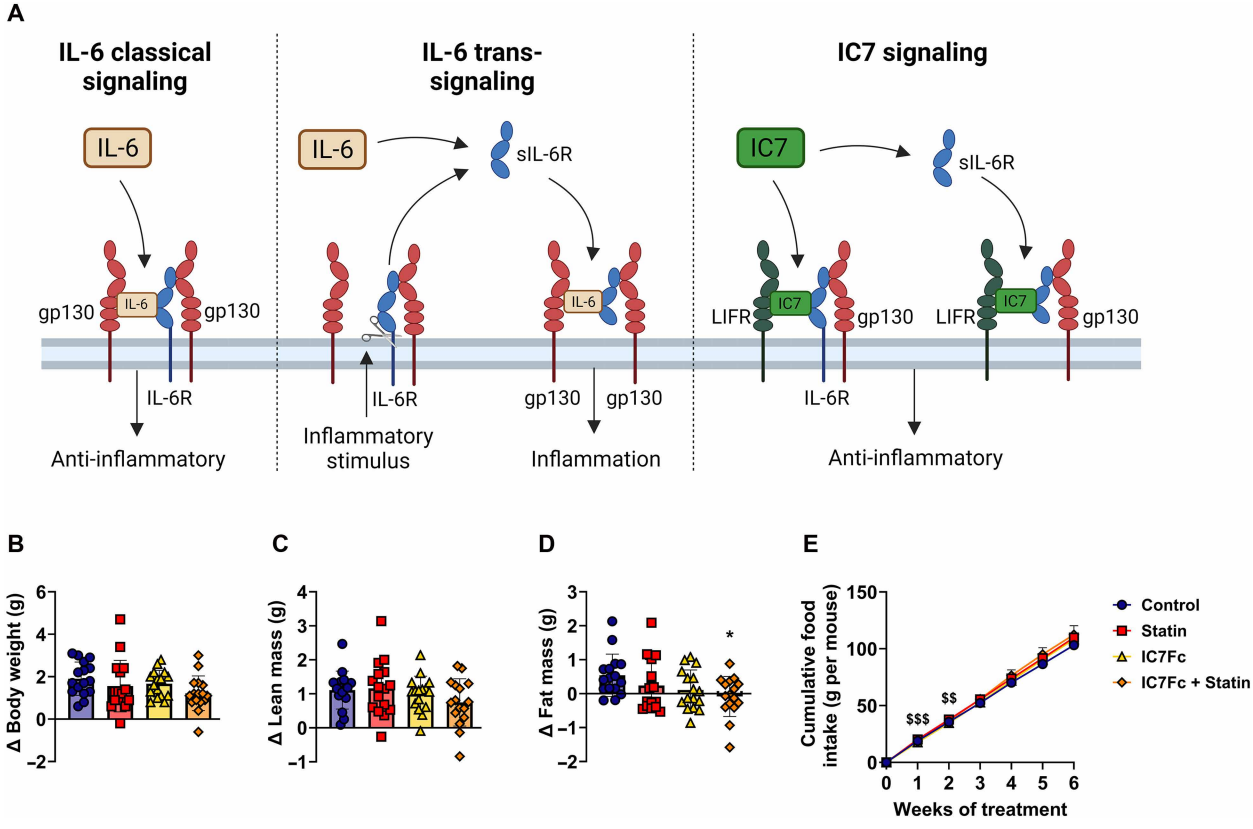

Fig. 1. Graphical illustration of IC7Fc signaling, and body composition and food intake. (**A**) Graphical illustration of interleukin-6 (IL-6) classical signaling, IL-6 trans-signaling, and IC7 signaling. Female APOE*3-Leiden.CETP mice were injected intraperitoneally twice weekly with IC7Fc (IC7Fc, yellow triangles) or vehicle (Control, blue circles) while receiving a high-cholesterol Western-type diet with or without the addition of atorvastatin (0.008%) (Statin, red squares; IC7Fc + Statin, orange diamonds) for a total duration of 7 weeks. (**B**) Body weight, (**C**) lean mass, and (**D**) fat mass were measured at weeks 0 and 7 from which delta change was calculated ($n = 15$ to 16 mice per group). Food intake was monitored weekly per cage ($n = 4$ cages of three to four mice per group) and expressed as (**E**) total food intake per mouse. Data are presented as means ± SD. *Any group versus Control; $^{\$}$Statin versus IC7Fc. $^{*}P < 0.05$, $^{\$\$}P < 0.01$, $^{\$\$\$}P < 0.001$, according to two-way ANOVA and following Tukey's multiple-comparison test. (A) Created in BioRender. In het Panhuis, W. (2025); https://BioRender.com/f1abs8c.

Downloaded from https://www.science.org at Leiden University on March 06, 2026

mice. The benefit of this model is that in contrast to other atherosclerosis mouse models, these mice respond well to widely used lipid-lowering medications such as statins and proprotein convertase subtilisin/kexin type 9 (PCSK9) inhibitors, as the APOE-LDLR interaction pathway for uptake of lipoprotein remnants by the liver is functionally intact in these mice (*24*–*27*). Accordingly, we compared the efficacy of our drug intervention, IC7Fc treatment, to the current antiatherosclerotic gold standard, statin therapy. Female APOE*3-Leiden.CETP mice were fed a high-cholesterol, Western-type diet (WTD) to induce hyperlipidemia with or without the addition of atorvastatin (0.008% w/w) to the diet and received two weekly intraperitoneal injections of IC7Fc (1 mg/kg in saline) or vehicle (saline) for a total duration of 7 weeks in a first experiment. The atorvastatin dose was chosen to mimic the effect in humans where moderately dosed atorvastatin treatment achieves a reduction in plasma cholesterol levels of approximately 30% (*28*, *29*). IC7Fc treatment modestly prevented the gain of fat mass over 7 weeks of treatment [IC7Fc effect by two-way analysis of variance (ANOVA): $P = 0.023$] alone and in combination with statin, without changing body weight, lean mass, or food intake (Fig. 1, B to E). Statin treatment alone did not alter body composition or food intake. At the cessation of the treatment period, atherosclerosis development in the aortic root of the heart was assessed. IC7Fc-treated mice had an 84% lower atherosclerotic lesion area on average compared with vehicle-treated control mice, while lesion size was on average 31% reduced in statin-treated mice (Fig. 2A and fig. S1A). Correspondingly, IC7Fc treatment resulted in a pronounced reduction in the amount of severe lesions and the complete prevention of lesion necrosis, and tended to reduce the relative lesion macrophage content while increasing the collagen and smooth muscle cell content, thereby increasing the lesion stability index (Fig. 2, B to G, and fig. S1A). In line, the lesion content of the proinflammatory markers CC chemokine receptor type 2 (CCR2) and endothelial intercellular adhesion molecule-1 (ICAM1) was significantly reduced by IC7Fc treatment (−61.5 and −58.5%, respectively) and the lesion content of vascular cell adhesion protein 1 (VCAM1) and the abundance of $CD3^+$ T cells tended to be reduced, altogether indicating reduced plaque inflammation (figs. S1A and S2, A to D). Combined statin and IC7Fc treatment did not further attenuate atherosclerosis progression compared with IC7Fc treatment alone, possibly because IC7Fc already potently attenuated atherosclerosis development, leaving little room for further improvement (Fig. 2, A to G, and fig. S1A).

IC7Fc treatment attenuates markers of tissue inflammation

To obtain mechanistic insight into the antiatherosclerotic treatment effect of IC7Fc, we first measured the expression of proinflammatory markers in the aorta. While the expression of *Icam1* was unchanged, IC7Fc reduced or tended to reduce the expression of *Vcam1*, *Ccr2*, and *Tnfa* (fig. S2, E to H; IC7Fc effect by two-way ANOVA: $P = 0.014$, 0.060, and 0.009, respectively) in line with the reduced relative macrophage content of the atherosclerotic lesions (Fig. 2D).

Next, we measured the relative abundance of circulating immune cell populations in blood collected at the study endpoint, including $CD4^+$ T helper cells, $CD8^+$ (cytotoxic T cells), and monocytes, which can be pro- or antiatherogenic depending on their subset (*30*, *31*). However, the relative abundance of these immune cell populations was unchanged between all groups (fig. S2, I to P). Accordingly, plasma levels of the inflammatory cytokines IL-6, IL-10, and TNF-α were unchanged (fig. S2, Q to S). These findings suggest that IC7Fc attenuates inflammation at the tissue level rather than systemically in this mouse model, which may be secondary to hyperlipidemia attenuation.

IC7Fc treatment greatly attenuates hyperlipidemia by reducing markers of hepatic lipid synthesis and lipoprotein secretion

To further investigate the underlying cause of the antiatherogenic effect of IC7Fc, we next assessed the impact of the treatment on hyperlipidemia. IC7Fc treatment markedly attenuated elevated plasma TG and total cholesterol (TC) levels (Fig. 2, H and J) as well as TG and TC exposure, i.e., the areas under the curve of TG and TC levels throughout the study that are predictive of atherosclerosis development (Fig. 2, I and K). The reduction in plasma TC was independent of changes in high-density lipoprotein cholesterol (HDL-c) levels (Fig. 2L). The atherosclerotic lesion area correlated with both TG and TC exposure, albeit to a larger extent to TC exposure, suggesting that IC7Fc reduces atherosclerosis development primarily by attenuating high plasma lipid levels (Fig. 2, M and N).

Next, we investigated the mechanism underlying the IC7Fc-induced improvement in hyperlipidemia by first quantifying cholesterol influx and efflux. For this, half of the mice received an oral bolus of [^{14}C]cholesterol at the study endpoint as a proxy measure of the intestinal uptake and tissue distribution of dietary cholesterol throughout the body. IC7Fc treatment did not alter the ^{14}C activity in the intestinal lumen, intestinal tissue, or peripheral tissues (fig. S3, A to M), suggesting no reduction in cholesterol absorption from the cholesterol-rich diet through the treatment. In contrast, statin treatment reduced hepatic [^{14}C]cholesterol uptake (statin effect by two-way ANOVA: $P = 0.014$) (fig. S3G). We next evaluated whether IC7Fc stimulated the reverse cholesterol transport pathway, a process by which cholesterol from the periphery, e.g., inside macrophages, is moved back to the liver and subsequently excreted. For this, the other half of the mice from all groups received an intraperitoneal injection of [1,2-^{3}H(N)]cholesterol–loaded murine macrophages from which the ^{3}H activity was traced into the feces over the following 4 days. Also here, fecal ^{3}H-derived activity was unchanged (fig. S3, N and O). Additional analyses of feces collected during week 5 of the experiment demonstrated that IC7Fc did not elevate the excretion of neutral sterols, i.e., cholesterol and its derivatives, or bile acids (fig. S4, A and B). IC7Fc tended to mildly increase fecal calorie excretion similarly to statin treatment (fig. S4C). Statin treatment also lowered the fecal excretion of neutral sterols in line with the known mechanism of action of statins to lower hepatic cholesterol synthesis.

Without an obvious mechanistic involvement of peripheral organs or pronounced effects on cholesterol absorption and excretion, we further investigated the effect of IC7Fc treatment on the regulation of lipid metabolism in the liver. For this, we measured the hepatic protein abundance of the key sensor of low cellular energy levels that inhibits de novo lipogenesis, AMP-activated protein kinase (AMPK), which is known to be activated by several members of the IL-6 family of cytokines including IC7Fc (*22*, *32*, *33*). Although IC7Fc treatment increased the p-AMPKα^{Thr172}/AMPKα ratio (fig. S4, D to F), suggesting a possibly transient increase in AMPK activity followed by a compensatory

Downloaded from https://www.science.org at Leiden University on March 06, 2026

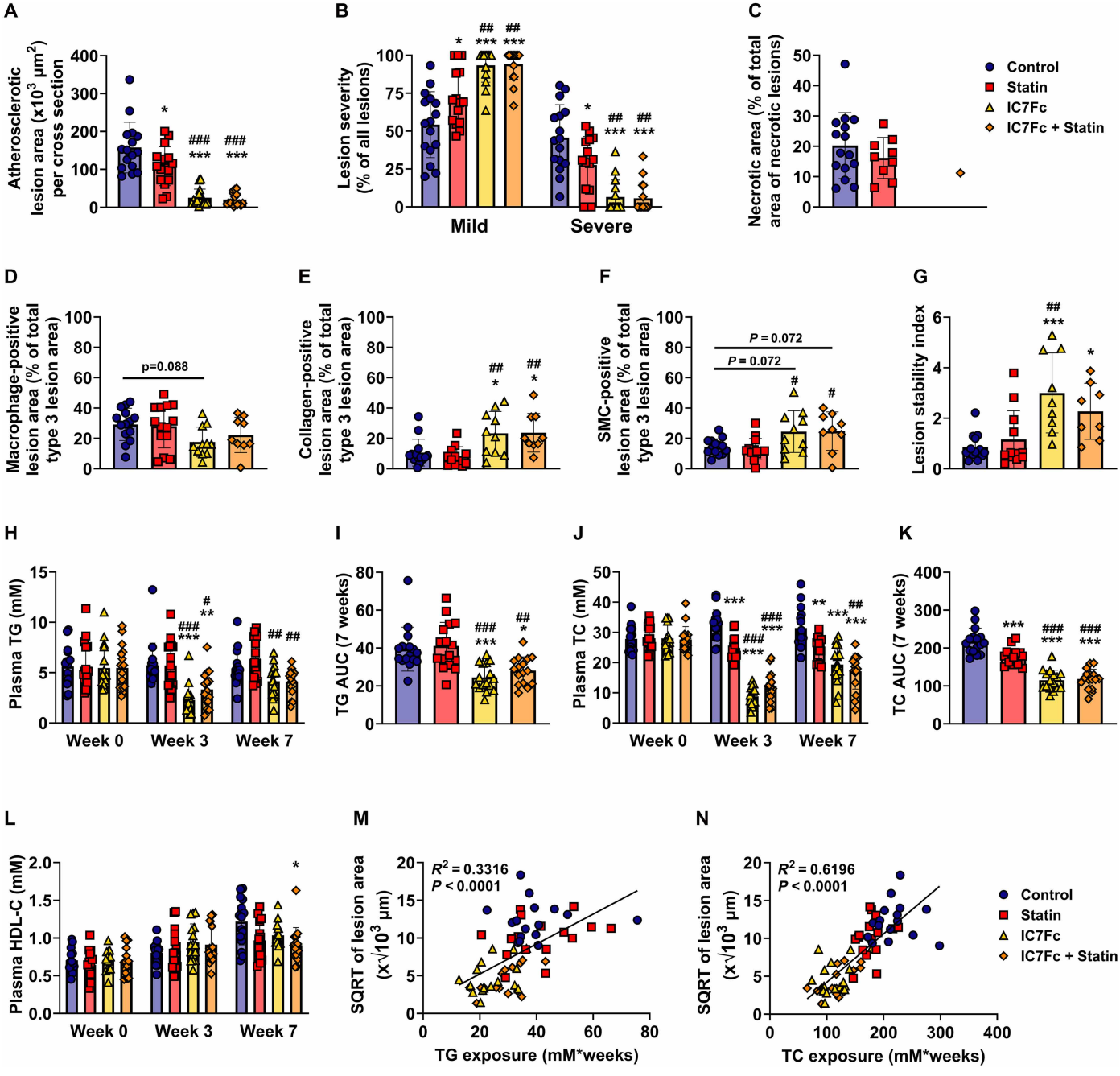

Fig. 2. IC7Fc treatment reduces atherosclerosis lesion area and severity and increases lesion stability index by profoundly improving hyperlipidemia. Cross sections of the aortic root area were stained with hematoxylin-phloxine-saffron and atherosclerotic lesion area was determined and expressed as a function of distance from the appearance of open aortic valves (**A**) from which the mean atherosclerotic lesion area was calculated. Lesions were categorized according to lesion severity, expressed as a percentage of total lesions, and shown (**B**) per lesion severity (mild, types I to III; severe, types IV and V) ($n = 15$ to 16 mice per group). (**C**) The necrotic core size in severe lesions with necrosis was measured. Cross sections were also stained using an anti-MAC-3 antibody, an α-actin antibody, or Sirius red staining to quantify the content of (**D**) macrophages, (**E**) collagen, and (**F**) smooth muscle cells (SMC), respectively ($n = 9$ to 16 mice per group). (**G**) Lesion stability index was calculated by dividing the sum of collagen and smooth muscle cell content by the macrophage content ($n = 8$ to 16 mice per group). Blood was collected to determine (**H**) plasma triglyceride levels (TG), (**I**) total TG exposure (AUC), (**J**) plasma total cholesterol levels (TC), (**K**) total TC exposure (AUC), and (**L**) high-density lipoprotein cholesterol (HDL-c) levels. Total (**M**) TG and (**N**) TC exposure were plotted against the square root (SQRT) of the mean atherosclerotic lesion area from which R and Pearson's correlation coefficients were determined ($n = 16$ per group). Data are presented as means ± SD. *Any group versus Control; $^{\#}$any group versus Statin. $^{*}P < 0.05$, $^{**,\#\#}P < 0.01$, $^{***,\#\#\#}P < 0.001$, according to one-way ANOVA [(A) to (G), (I), and (K)] or two-way ANOVA [(H), (J), and (L)] and following Tukey's multiple-comparison test.

Downloaded from https://www.science.org at Leiden University on March 06, 2026

down-regulation of total AMPKα over 7 weeks of treatment, total and phosphorylated levels of downstream target acetyl-CoA carboxylase (ACC) that regulates fatty acid synthesis were unchanged (fig. S4, G to I). Nonetheless, IC7Fc, but not statin treatment, after 7 weeks reduced or tended to reduce the expression of genes involved in de novo lipogenesis [i.e., liver X receptor (LXR, gene name *Nr1h3*), sterol regulatory element-binding protein 1c (SREBP1c, gene name *Srebf1*), and ACC (gene name *Acaca*)] and VLDL production [i.e., apolipoprotein B (*Apob*) and microsomal TG transfer protein (*Mttp*)] (Fig. 3, A to C, E, and F), indicating that these effects are independent of AMPK activation at study endpoint. Instead, IC7Fc treatment lowered plasma insulin levels, suggesting increased insulin sensitivity (Fig. 3D). In line, IC7Fc, but not statin treatment, reduced the hepatic gene expression of sterol regulatory element-binding protein 2 (*Srebp2*) and low-density lipoprotein receptor (*Ldlr*), but without altering 3-hydroxy-3-methyl-glutaryl-coenzyme A reductase (*Hmgcr*) expression (fig. S4, J to L). In addition, IC7Fc treatment reduced the expression of the transcription factors involved in the transcriptional regulation of *Apob* (*34*), NR2F2 (also known as ARP-1) and HNF4α (Fig. 3, G and H).

Collectively, these data indicate that IC7Fc attenuates hyperlipidemia by lowering de novo lipogenesis and VLDL production in the liver. To further investigate the underlying cause of the effect seen in vivo, we focused on the mechanism of action of IC7Fc and did not include the comparison with statin treatment in the following experiments.

IC7Fc treatment lowers VLDL secretion without altering cholesterol synthesis

Because gene expression analyses suggested that IC7Fc treatment lowers hepatic VLDL secretion, VLDL-TG production rate as well as VLDL-apolipoprotein B (APOB) production were assessed in a follow-up experiment. APOE*3-Leiden.CETP mice were treated with IC7Fc or vehicle for 3 weeks, and we confirmed that IC7Fc treatment robustly lowered plasma lipid levels (fig. S5, A and B). IC7Fc treatment caused a pronounced reduction in hepatic TG production and VLDL-TG and VLDL-TC content (Fig. 4, A to C) with a corresponding reduction in VLDL-[^{35}S]APOB production (Fig. 4D). VLDL-TG/APOB ratio was unchanged (Fig. 4E), indicating a reduced number of VLDL particles rather than reduced particle lipidation. The attenuation of lipogenesis appeared to be an indirect effect on the liver because IC7Fc treatment did not directly lower lipogenesis in HepG2 cells, measured by quantifying the incorporation of [^{14}C]palmitic acid into lipids in vitro (fig. S5C). However, using a genome-engineered human-derived HepG2 cell line expressing endogenous fluorescent APOB (*35*), we confirmed that IC7Fc down-regulates both intracellular and secreted APOB levels directly in hepatocytes (fig. S5, D and E). In these cells, we also confirmed that acute IC7Fc treatment induces the phosphorylation of signal transducer and activator of transcription 3 (STAT3) in the activation cascade of the IL-6R/JAK/STAT signaling pathway, as shown previously (*22*) (fig. S5F). In primary murine hepatocytes that were cotreated with IC7Fc and the HNF4α agonist N-trans-caffeoyltyramine (NCT), we observed that the IC7Fc-induced reduction

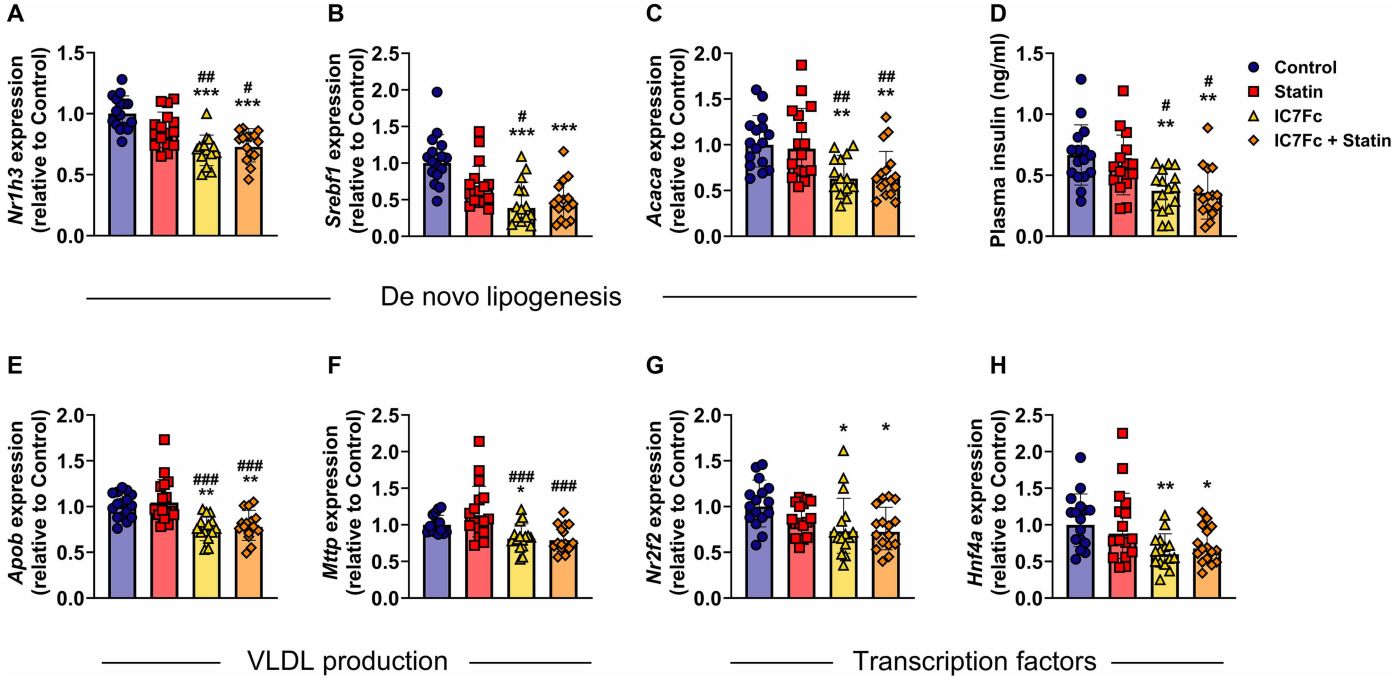

Fig. 3. IC7Fc treatment reduces hepatic markers of de novo lipogenesis and very low–density lipoprotein (VLDL) production. Expression of genes involved in lipid sensing and de novo lipogenesis [(**A**) liver X receptor (LXR, gene name *Nr1h3*), (**B**) sterol regulatory element-binding protein 1c (SREBP1c, gene name *Srebf1*), and (**C**) acetyl-CoA carboxylase (ACC, gene name *Acaca*)] was measured in liver tissue after 7 weeks of treatment ($n = 14$ to 16 per group) as well as (**D**) fasted plasma insulin levels at the end of the treatment period. Gene expression of genes involved in VLDL production [(**E**) apolipoprotein B (*Apob*) and (**F**) microsomal triglyceride transfer protein (*Mttp*)] and related transcription factors (**G**) *Nr2f2* and (**H**) *Hnf4a* was also measured in liver ($n = 14$ to 16 per group). Gene expression data are presented as geometric means ± geometric SD. Insulin data are shown as means ± SD. *Any group versus Control; #any group versus Statin; *,#$P < 0.05$, **,##$P < 0.01$, ***,###$P < 0.001$, according to two-way ANOVA and following Tukey's multiple-comparison test.

Downloaded from https://www.science.org at Leiden University on March 06, 2026

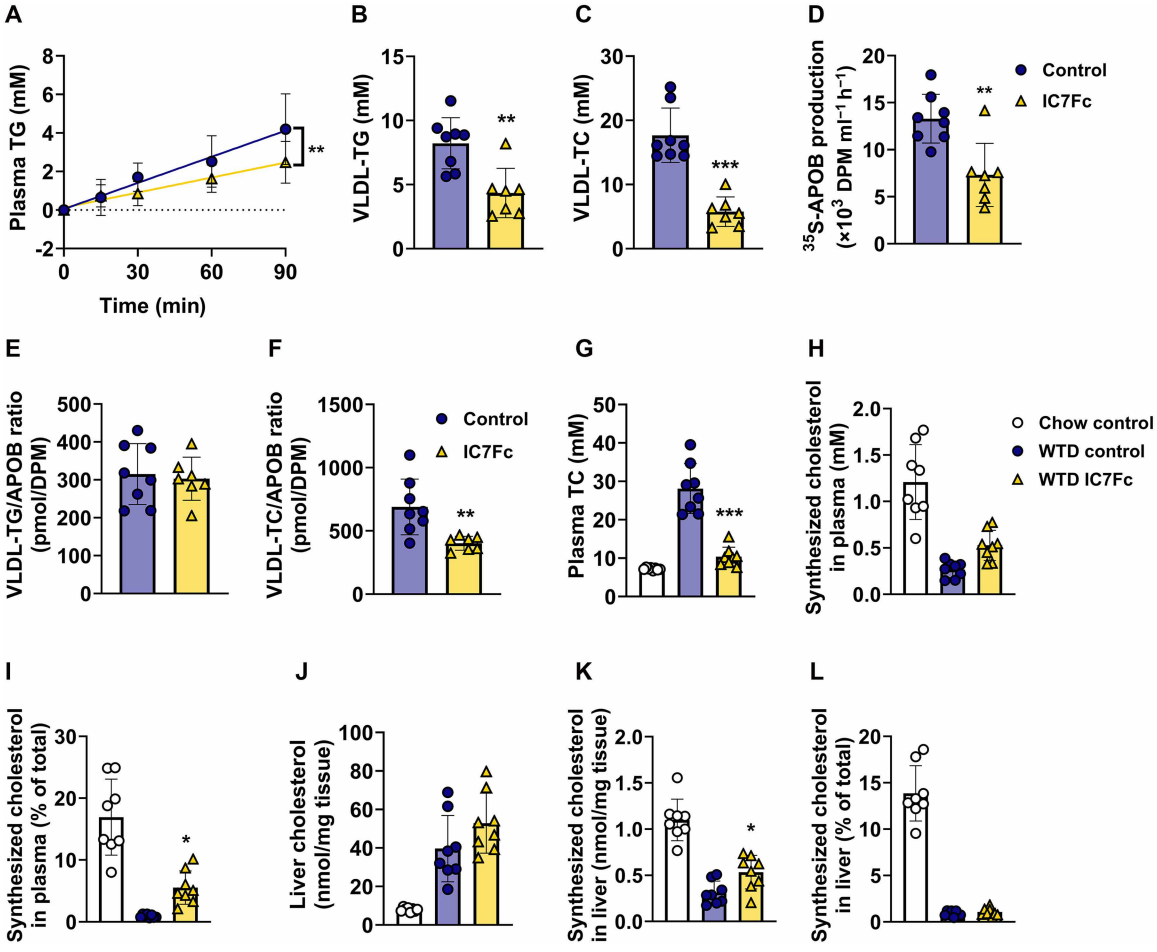

Fig. 4. IC7Fc treatment down-regulates VLDL production, without altering cholesterol synthesis. Female APOE*3-Leiden. CETP mice were injected intraperitoneally twice weekly with IC7Fc (IC7Fc, yellow triangles) or vehicle (Control, blue circles) while receiving a high-cholesterol Western-type diet for a total duration of 3 weeks. After 3 weeks, mice were injected with Tran[^{35}S] label followed by Triton WR1339, and triglyceride (TG) levels were determined in plasma samples drawn at the indicated time points, which were (**A**) plotted as the increase in TG to baseline, from which VLDL-TG production rate was determined by linear regression. Concentrations of (**B**) TG and (**C**) total cholesterol (TC) within VLDL particles were measured and corrected for the total volume of isolated VLDL. (**D**) Apolipoprotein B (APOB) production was determined by measuring ^{35}S in isolated VLDL, from which the ratio of (**E**) VLDL-TG and (**F**) VLDL-TC over APOB was calculated ($n = 7$ to 8 mice per group). A different cohort of mice, which included a chow-fed vehicle group (Chow control) in addition to a Western-type diet (WTD)–fed vehicle (WTD control) and WTD-fed IC7Fc group (WTD IC7Fc), received 5% deuterated drinking water during the last 3 days of 3 weeks of treatment. (**G** to **I**) Plasma and (**J** to **L**) liver collected at endpoint; [(G) and (J)] unlabeled and [(H) and (K)] deuterium-labeled cholesterol was measured, from which the percentage of deuterium-labeled cholesterol [(I) and (L)] was calculated ($n = 8$ mice per group). Data are presented as means ± SD. *IC7Fc versus WTD vehicle. $^{**}P < 0.01$, $^{***}P < 0.001$, according to linear regression (A), unpaired *t* test [(B) to (F)], or one-way ANOVA and following Šídák's multiple-comparison test [(G) to (L)].

in gene expression of VLDL production-associated genes was counteracted by NCT treatment, suggesting involvement of HNF4α in the IC7Fc signaling effect (fig. S5, G to J).

In contrast to the unchanged VLDL-TG/APOB ratio, the VLDL-TC/APOB ratio was decreased in vivo (Fig. 4F), suggesting that reduced VLDL particle production was accompanied by lower incorporation of cholesteryl esters in the particles. To study whether reduced hepatic cholesterol synthesis could further explain this reduced cholesterol incorporation into VLDL, we treated another cohort of mice with IC7Fc or vehicle for 3 weeks and replaced the drinking water with 5% $^{2}H_2O$ water for the last 3 days of the study to measure deuterium-labeled and unlabeled cholesterol in plasma and liver. As a reference point for hepatic cholesterol synthesis levels on a low- and high-cholesterol diet, a group of healthy chow-fed mice was included in this experiment along with a control group on WTD. We confirmed a reduction in plasma lipid levels with IC7Fc compared with the WTD control group (Fig. 4G and fig. S6, A and B). IC7Fc treatment lowered the expression of *Hmgcr* and phosphomevalonate kinase (*Pmvk*) and increased the expression of mevalonate kinase (*Mvk*), genes involved in the cholesterol synthesis pathway (fig. S6, C to E). Unexpectedly, cholesterol synthesis as measured with deuterium labeling was, however, unchanged (Fig. 4H). As the plasma total cholesterol level was reduced with IC7Fc and the plasma level of deuterium-labeled cholesterol was unchanged, the percentage of newly synthesized labeled cholesterol in the plasma was consequently elevated (Fig. 4I). In the liver, the concentration of total cholesterol was unaltered but total labeled cholesterol was increased, albeit without significantly elevating the

Downloaded from https://www.science.org at Leiden University on March 06, 2026

relative abundance of newly synthesized cholesterol in the hepatic cholesterol pool (Fig. 4, J to L). These data suggest that IC7Fc treatment lowers plasma TG and TC levels by lowering the secretion of VLDL particles, which is, however, not associated with reduced hepatic cholesterol synthesis. Staining of the liver tissue for neutral lipids did not show a significantly increased hepatic lipid accumulation with IC7Fc treatment (fig. S6, F and G). Accordingly, 7 weeks of IC7Fc treatment did not induce liver steatosis (fig. S6, H and I) but mildly elevated the hepatic total cholesterol content and combined treatment with IC7Fc and statin mildly elevated the hepatic TG content (fig. S6, J and K). However, IC7Fc did not affect the hepatic gene expression of macrophage markers (*Ly6c* and *Adgre1*) or proinflammatory cytokines (*Mcp1*, *Il1b*, and *Tnfa*) compared with the control group (fig. S6, L and P). These data indicate that IC7Fc treatment does not induce liver inflammation, despite a mild elevation in hepatic cholesterol content over a longer treatment period in APOE*3-Leiden.CETP mice.

IC7Fc treatment lowers plasma cholesterol levels by altering hepatic bile acid metabolism

We hypothesized that the reduced cholesteryl ester incorporation into VLDL is a consequence of higher hepatic bile acid synthesis from cholesterol. We therefore measured the hepatic concentration of the bile acid synthesis intermediate 7-alpha-hydroxy-4-cholesten-3-one (C4), which was indeed increased by IC7Fc treatment along with liver and plasma total bile acid levels (Fig. 5, A to C). Correspondingly, IC7Fc lowered the expression of the hepatic bile acid transporters Na^+ taurocholate cotransporting polypeptide (NTCP) (gene name *Slc10a1*), organic anion transporting polypeptide (OATP)1A1 (gene name *Slco1a1*), OATP1A4 (gene name *Slcp1a4*), and OATP1B2 (gene name *Slc01b2*) (Fig. 5, D to G), suggesting that reduced hepatic bile acid uptake transport capacity caused a delay in the clearance of plasma bile acids. Furthermore, the hepatic expression of the bile acid–sensing farnesoid X receptor (FXR, gene name *Nr1h4*) was reduced (Fig. 5H). While the expression of the FXR target gene nuclear Receptor Subfamily 0 Group B Member 2 (SHP, gene name *Nr0b2*) was not altered, the transcriptional repressor of bile acid synthesis MAF bZIP transcription factor G (*Mafg*) and the ATP Binding Cassette Subfamily B Member 11 (BSEP, gene name *Abcb11*) that functions as a hepatic bile acid exporter were reduced upon IC7Fc treatment (Fig. 5, I to K). The gene expression of *Slco1a1*, *Slco1a4*, and *Bsep* was also down-regulated in vitro in primary hepatocytes upon IC7Fc treatment (fig. S5, K to M), suggesting this effect to be direct. Together, these data support the hypothesis that the modulation of hepatic bile acid metabolism contributes to the reduction in plasma lipid levels that underlie the antiatherosclerotic effect of IC7Fc.

DISCUSSION

The modulation of IL-6 signaling is a promising target for the treatment of CVD. Here, we demonstrate that IC7Fc, a chimeric molecule that activates the signaling pathway of IL-6 by binding the heterotrimeric LIFR–(s)IL-6R–gp130 receptor complex and that ameliorates obesity and T2DM (*22*), profoundly attenuates hyperlipidemia and atherosclerosis development in humanized atherosclerosis-prone APOE*3-Leiden.CETP mice.

In obese mice, IC7Fc was previously found to suppress appetite via the stimulation of the incretin response and consequently reduce body weight and fat mass (*22*). We here observed that lean hyperlipidemic APOE*3-Leiden.CETP mice maintained their body mass and food intake was not affected by IC7Fc treatment. Unlike obese mice, APOE*3-Leiden.CETP mice on a WTD have an intact incretin system and are, therefore, likely less responsive to an additional induction of GLP-1 secretion through IL-6R activation in the intestine (*36*, *37*). In addition, we studied female APOE*3-Leiden.CETP mice here that are atherosclerosis prone but at the same time less obesity prone than males. Together, IC7Fc may reduce appetite and fat mass particularly in obesity while lean individuals may likely still benefit from the antiatherosclerotic effect. These findings warrant further (clinical) investigations.

IC7Fc very effectively reduced the development of atherosclerotic lesions, lesion severity and necrosis, and local inflammation. This indicates the potential for this designer cytokine to close the therapeutic gap left in the treatment of CVDs with current drugs. This also demonstrates that both the previously studied inhibition of IL-6 signaling or trans-signaling and the activation of the IL-6 signaling pathway can improve atherosclerotic outcomes. Uniquely, however, IC7Fc simultaneously robustly lowered plasma TG and non-HDL cholesterol levels, which are both independent risk factors for the development of atherosclerotic CVD (*4*, *38*). This unexpected biological activity of IC7Fc may be associated with its binding to a receptor complex [LIFR–(s)IL-6R–gp130] that is not engaged by any natural cytokines. In addition, whereas the circulating IL-6–sIL-6R complex can be neutralized by endogenous sgp130, IC7Fc is not prone to such buffering, which may modulate its signaling efficacy compared to endogenous IL-6 (*22*). The antihyperlipidemic effect of IC7Fc treatment seems more potent after 3 weeks than after 7 weeks of treatment. This is likely not related to autoantibody formation, because IC7Fc does not induce immunogenicity in nonhuman primates and human peripheral blood mononuclear cells (*22*). A potential explanation is that the reduction in fat mass increases free fatty acid flux from white adipose tissue toward the liver, which may stimulate hepatic VLDL secretion compared to the initial reduction seen after 3 weeks. Reduced fat mass may also attenuate clearance of TG-rich lipoprotein remnants from the circulation. These effects combined with the persistent influx of diet-derived cholesterol may gradually increase TG and TC. Nonetheless, the reduction in plasma lipids in week 7 remains profound and potentially clinically relevant. In contrast to the antihyperlipidemic effect of IC7Fc treatment, IL-6 gain-of-function polymorphisms in humans that result in increased IL-6 secretion and the administration of exogenous IL-6 in rodents have been linked to elevated plasma lipid levels, which may be a consequence of induced IL-6 trans-signaling (*39*–*42*).

Our data point toward the liver as the primary organ responsible for the reduction in plasma lipid levels as reduced hepatic VLDL secretion is in line with lowered markers of hepatic de novo lipogenesis and increased conversion of cholesterol into bile acids. Mechanistically, IC7Fc treatment transiently increased AMPK activity in accordance with previous studies (*22*, *43*), which attenuates hepatic de novo lipogenesis (*22*) and stimulates hepatic bile acid synthesis through the inhibition of FXR signaling (*32*). However, as AMPK activity was normalized after 7 weeks of IC7Fc treatment following a compensatory down-regulation of AMPKα protein levels, it may also have contributed to the stronger lipid-lowering effect in week 3 versus week 7, but it cannot explain the prolonged lipid-lowering effects observed here. Instead, IC7Fc treatment also lowered circulating

Downloaded from https://www.science.org at Leiden University on March 06, 2026

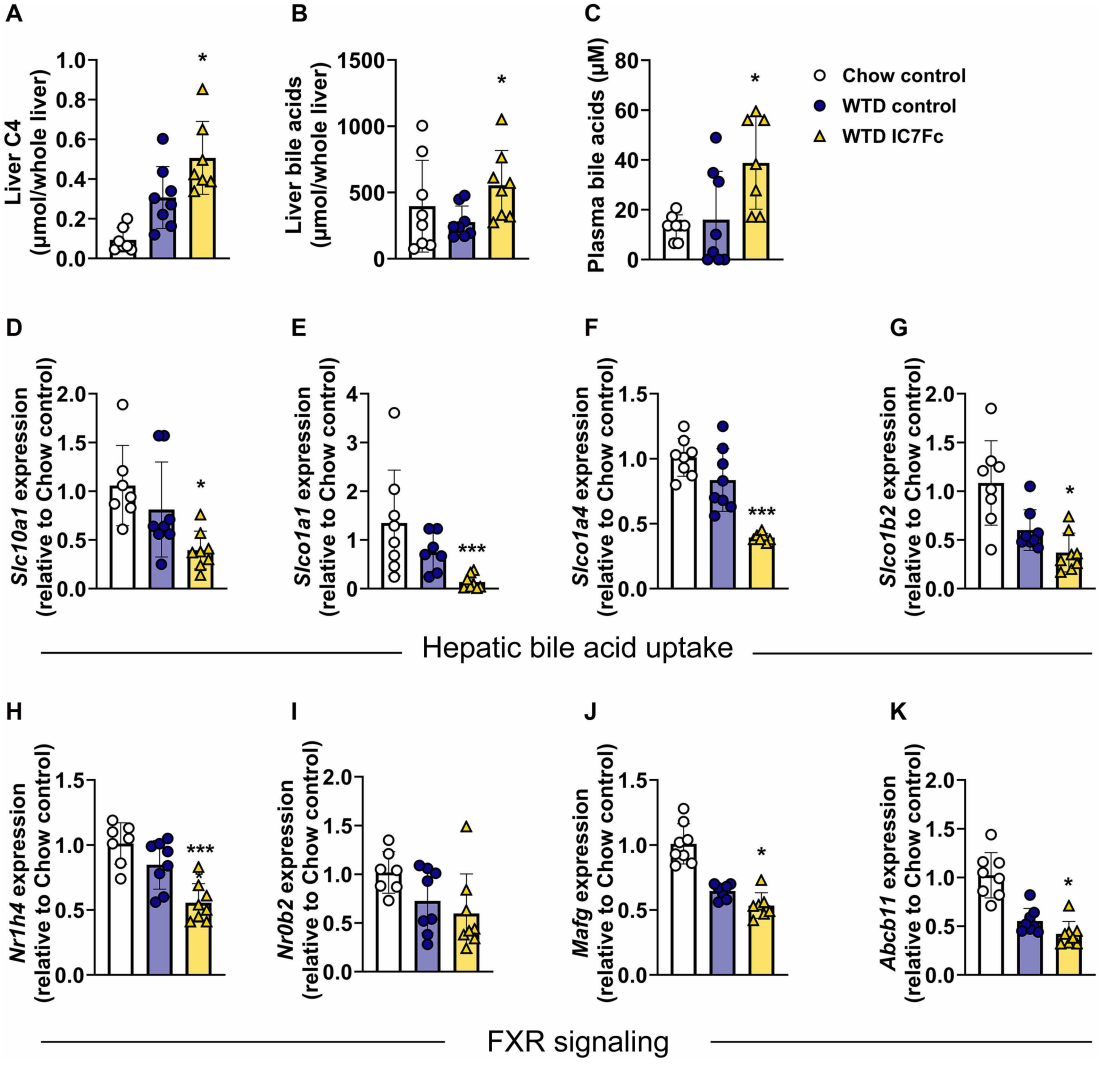

Fig. 5. IC7Fc treatment increases bile acid synthesis and plasma bile acid levels. After 3 weeks of treatment, bile synthesis intermediate (**A**) 7-alpha-hydroxy-4-cholesten-3-one (C4) was measured and expressed per whole liver. (**B**) Total bile acid levels were measured in the liver and in (**C**) plasma collected after 3 weeks of treatment. Expression of genes involved in bile acid uptake [(**D**) Na^+ taurocholate cotransporting polypeptide (NTCP, gene name *Slc10a1*), (**E**) organic anion transporting polypeptide 1a1 (OATP1A1, gene name *Slco1a1*), (**F**) OATP1A4 (gene name *Slco1a4*), and (**G**) OATP1B2 (gene name *Slco1b2*)] and bile acid signaling [(**H**) farnesoid X receptor (*Fxr*), (**I**) nuclear Receptor Subfamily 0 Group B Member 2 (SHP, gene name *Nr0b2*), (**J**) MAF bZIP transcription factor G (*Mafg*), and (**K**) ATP Binding Cassette Subfamily B Member 11 (BSEP, gene name *Abcb11*)] was measured in liver after 3 weeks of treatment ($n = 7$ to 8 mice per group). Data are presented as means ± SD. *IC7Fc versus WTD control. $^*P < 0.05$, $^{***}P < 0.001$, according to one-way ANOVA and following Šídák's multiple-comparison test.

insulin levels, indicating improved insulin sensitivity as described previously (*22*), which aligns with reduced de novo lipogenesis and VLDL secretion (*44*). Because insulin resistance promotes atherosclerosis development, IC7Fc treatment may also protect against atherosclerosis through improved insulin sensitivity (*45*). HNF4α, a crucial transcription factor in the regulation of hepatic lipid and bile acid homeostasis, was down-regulated by IC7Fc as previously observed with the activation of the IL-6 signaling pathway (*46*). As also seen with IL-6 signaling (*47*), down-regulation of *Hnf4a* gene expression decreased the expression of *Apob*, *Mttp*, and hepatic bile acid transporters, resulting in reduced VLDL secretion and increased plasma bile acids, respectively (*48*). Particularly in obese mouse models, this corresponding increase in plasma bile acid levels was formerly shown to protect against cardiometabolic diseases by increasing systemic bile acid signaling (*49*–*51*). These signaling effects range from the attenuation of weight gain and improved glucose tolerance to increased incretin secretion and align with the response of obese animals to IC7Fc treatment. In humans, a loss-of-function single-nucleotide polymorphism (SNP) in the *SLC10A1* gene (S267F), encoding NTCP, was found to be associated with elevated plasma bile acid levels without negative effects, and lowered plasma cholesterol levels (*52*). Last, IC7Fc treatment promoted a moderate accumulation of lipids in the liver, which possibly also contributed to the profoundly reduced plasma lipid levels. However, this lipid accumulation is not observed in other mouse models (*22*). Our findings are summarized in Fig. 6.

The current clinical development of IL-6–targeted drugs focus either on the inhibition of circulating IL-6 or the inhibition of

Downloaded from https://www.science.org at Leiden University on March 06, 2026

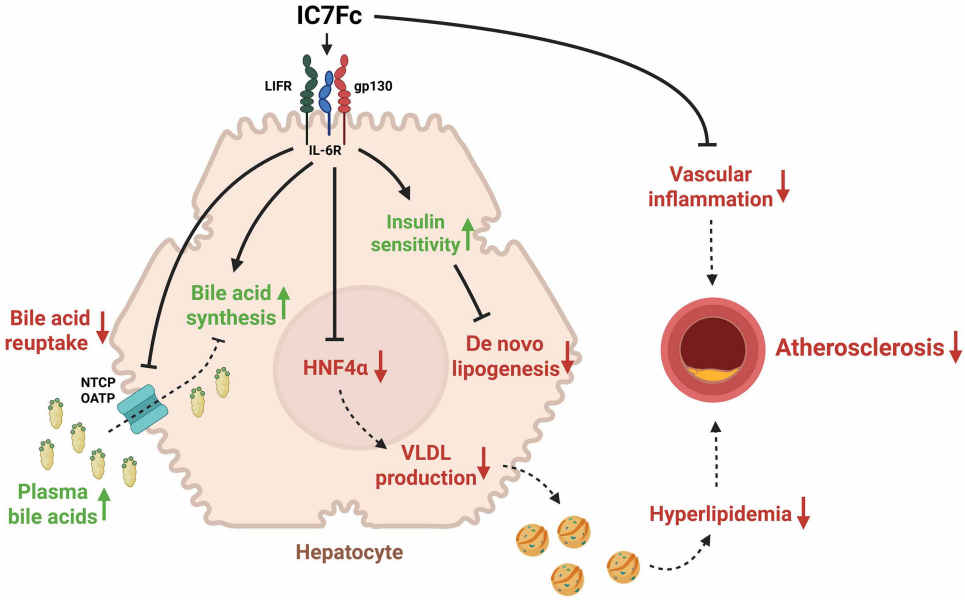

Fig. 6. IC7Fc ameliorates atherosclerosis development through the modulation of hepatic lipid metabolism. IC7Fc signaling lowers hepatic de novo lipogenesis and modulates bile acid metabolism, which increases plasma bile acid levels following reduced hepatic reuptake of bile acids. The inhibition of transcription factor HNF4α contributes to the reduced synthesis and secretion of APOB-containing VLDL particles. This leads to the attenuation of hyperlipidemia and atherosclerosis development. gp130, coreceptor glycoprotein 130; IL-6R, interleukin-6 receptor; LIFR, leukemia inhibitory factor receptor. Solid lines, up-regulated process; dashed lines, down-regulated process; green arrow, up-regulated; red arrow, down-regulated. Created in BioRender. In het Panhuis, W. (2025); https://BioRender.com/klk4s79.

trans-signaling specifically. Namely, the IL-6 monoclonal antibody ziltivekimab is entering a large-scale phase 3 cardiovascular outcomes trial (NCT05021835) (*11*) after anti-inflammatory outcomes were reported in two phase 2 trials (*11*, *53*). In addition, the inhibition of trans-signaling, using an sgp130Fc protein called olamkicept that sequesters the circulating IL-6–sIL-6R complex (*54*), has passed phase 2 clinical trials for the treatment of inflammatory bowel disease and ulcerative colitis (*17*, *55*). Given that the inhibition of trans-signaling was formerly shown to attenuate atherosclerosis development in mice (*56*) and arterial wall inflammation in a patient with a very high risk for cardiovascular events (*57*), the application of olamkicept may extend to CVD. However, neither the global inhibition of IL-6 nor the inhibition of trans-signaling counteracts hyperlipidemia as seen here with the treatment of IC7Fc that also conveyed anti-inflammatory properties, likely owing to its noninnate receptor complex formation. In conclusion, IC7Fc is a promising treatment candidate for inflammatory and lipid-driven diseases like atherosclerosis and should also be investigated further in the context of autoimmune disorders and metabolism dysfunction-associated steatotic liver disease.

MATERIALS AND METHODS

Animals

All experiments were performed in accordance with the Institute for Laboratory Animal Research Guide for the Care and Use of Laboratory Animals and were approved by the National Committee for Animal experiments (AVD11600202010187). Female APOE*3-Leiden.CETP mice that develop hyperlipidemia and atherosclerosis to a far greater extent than their male counterparts when fed a cholesterol-rich WTD (*25*, *26*, *58*, *59*) were generated as previously described (*23*). APOE∗3-Leiden.CETP mice express a naturally occurring mutant form of human APOE3, causing delayed clearance of atherogenic lipoprotein remnants by the liver (*23*, *25*), and a transgene for human cholesteryl ester transfer protein (CETP), which allows for transfer of cholesteryl esters from high-density lipoprotein (HDL) to low-density lipoprotein (LDL) particles and for which rodents are naturally deficient. As a result, female APOE*3-Leiden.CETP mice have a human-like lipoprotein metabolism and develop hyperlipidemia and atherosclerosis when fed a cholesterol-rich diet.

All mice were housed in groups of two to four mice per cage under standard conditions with 12-hour light/12-hour dark cycles at 21°C. Three weeks before the start of the intervention, mice were switched from standard chow diet (Rat and Mouse No. 3 Breeding, SDS, Horley, United Kingdom) to WTD (16% fat; 0.40% cholesterol; Diet T; Ssniff-Spezialdiäten GmbH, Soest, Germany), which they received ad libitum throughout the intervention, unless indicated otherwise. The intervention consisted of two weekly intraperitoneal injections with IC7Fc [1 mg/kg in saline (*22*)] or vehicle (saline). In all experiments, body weight, body composition (EchoMRI 100-Analyzer; EchoMRI, Houston, Texas), and food intake were monitored at regular intervals, and blood was collected from the tail vein at indicated time points to measure plasma lipid levels.

In the first experiment, mice were treated for a total duration of 7 weeks with IC7Fc or vehicle and received WTD with or without the addition of atorvastatin (0.008% w/w in the diet; TEVA), of which the dosage was based on dose finding studies to mimic the effect in humans where statin treatment achieves a reduction in plasma cholesterol levels of approximately 30%. The resulting four experimental groups ($n = 16$ per group) were therefore defined as Control, Statin, IC7Fc, and IC7Fc + Statin. During week 5, mice were single-housed for 48 hours for feces collection. During week 7, intestinal cholesterol absorption and tissue distribution was assessed

Downloaded from https://www.science.org at Leiden University on March 06, 2026

in half of the mice ($n = 8$ per group), and reverse-cholesterol transport was assessed in the other half of mice. At the study endpoint, blood was collected to measure circulating immune cells and cytokines. Mice were killed at Zeitgeber Time 6 (ZT6; i.e., 6 hours into the light phase) with CO_2 and subsequently perfused transcardially with ice-cold phosphate-buffered saline (PBS) for 5 min before tissues were collected for further analyses.

In a second experiment, mice were treated with IC7Fc or vehicle for 3 weeks and the resulting two experimental groups ($n = 8$ per group) were therefore defined as Control and IC7Fc. After 3 weeks, mice were injected with a radioactive label to assess APOB production and a lipoprotein lipase (LPL) inhibitor to assess hepatic VLDL production at ZT6.

In a third experiment, mice were treated with IC7Fc or vehicle for 3 weeks and an additional group was included that was not switched to WTD, but instead continued to receive standard chow diet. The resulting three experimental groups ($n = 8$ per group) were therefore defined as Chow control, WTD control, and WTD IC7Fc. During week 3, the drinking water of these mice was replaced by water with 5% ^2H_2O for 3 days, after which mice were killed with CO_2, cardiac puncture blood was collected, and the mice were subsequently perfused transcardially with ice-cold PBS for 5 min before livers were collected to assess hepatic cholesterol synthesis at ZT12.

Cell culture

HepG2 cells were obtained from the American Type Culture Collection (ATCC; Manassas, VA, USA) and were cultured in Dulbecco's modified Eagle's medium (DMEM) supplemented with 10% fetal bovine serum (FBS) and penicillin-streptomycin (10,000 U/ml; Thermo Fisher Scientific, MA, USA). All cells were grown in a humidified environment at 37°C and 5% CO_2.

Endogenously tagged HepG2-APOB-mNeon cells were generated for the assessment of APOB production and secretion. The generation and functional validation of these cells have been recently described by Meurs *et al.* (*35*). To evaluate the intracellular regulation and subsequent secretion of APOB, the cells were treated with IC7Fc (100 ng/ml) for 1 hour or 24 hours, respectively. Vehicle control was used in all experiments. The description of the quantification of intracellular APOB-mNeon can be found in the "Flow cytometry" section. For protein quantification, cells were stimulated with IC7Fc (100 ng/ml) or vehicle for 30 min.

To measure the secretion of fluorescent APOB-mNeon–containing lipoproteins, culture media was removed and replaced with FluoroBrite DMEM (Thermo Fisher Scientific). Medium was collected and cleared by centrifugation at 4°C for 5 min at 10,000*g*. Fluorescence intensity in the cleared medium was measured using a CLARIOstar plate reader (BMG LABTECH, Ortenberg, Germany) with excitation set at 492 nm and emission detection at 537 nm. Basal fluorescence in culture media was subtracted to account for background fluorescence signal.

Effects on transcription factor regulation were assessed in primary murine hepatocytes. For this, hepatocytes were isolated from a 12-week-old male C57BL/6J mouse using a two-step collagenase perfusion method through the portal vein as previously described (*60*). Cells were plated at 1.5×10^5 cells/cm^2 in a 24-well plate for protein analysis and in a 48-well plate for gene expression analysis. Primary hepatocytes were cultured in DMEM supplemented with glucose (4.5 g/liter), 1 mM L-glutamine, penicillin (37.5 U/ml), streptomycin (37.5 mg/ml), sodium bicarbonate (1.75 g/liter), and 20 mM 4-(2-hydroxyethyl)-1piperazine ethanesulfonic acid (pH 7.4). Upon isolation, cells were incubated for 4 hours (5% CO_2 at 37°C) in medium with Bodinco 10% FBS (BioWest, Nuaillé, France) followed by overnight incubation in medium deprived of serum. Subsequently, cells were stimulated with IC7Fc (100 ng/ml), HNF4α agonist N-trans-caffeoyltyramine (NCT, 5 μM, MedChemExpress, NJ, USA), both, or vehicle [0.4% dimethyl sulfoxide (DMSO)] for 2 hours for gene expression analyses.

Lipogenesis was assessed in HepG2 cells. On the evening before initiating the lipogenesis assay, cells were washed twice with prewarmed PBS and incubated overnight (~16 hours) at 37°C in serum starvation medium supplemented with 100 nM human insulin to prime lipogenesis. On the day of the experiment, cells were incubated in lipogenesis medium, consisting of serum starvation medium [DMEM with glucose (1 g/liter)] supplemented with 0.5 mM palmitate (Sigma-Aldrich, St. Louis, USA) conjugated to 2% fatty acid–free bovine serum albumin (BSA; Bovogen, Melbourne, Australia), and 0.2 μCi per well of [1-^{14}C]palmitic acid (NE075H050UC, Perkin Elmer, Waltham, MA, USA). Cells were treated with either IC7Fc (100 ng/ml) or IgGFc (100 ng/ml; Assay Matrix, Melbourne, Australia) and incubated at 37°C for 4 or 24 hours. Following the treatment period, cells were washed three times with ice-cold PBS and passed through a 30G insulin syringe four times and lysed by scraping in 200 μl of PBS. A 10-μl aliquot was reserved for protein quantification using the bicinchoninic acid (BCA) assay (Thermo Fisher Scientific, Waltham, MA, USA). The remaining 190 μl of lysate was transferred to a 1.5-ml microcentrifuge tube and frozen at −20°C overnight.

The following day, lipids were extracted by adding 600 μl of chloroform:methanol (2:1, v/v) to the thawed lysate. Samples were vortexed briefly and incubated at room temperature for 5 min before adding 250 μl of water and vortexing again. After an additional 5-min incubation at room temperature, samples were centrifuged at 3000*g* for 10 min. The lower (organic) phase (~350 μl) was carefully collected and transferred to scintillation vials containing 4 ml of liquid scintillation fluid (Ultima Gold, Perkin Elmer, Waltham, MA, USA). Incorporated [^{14}C]palmitic acid activity was measured by liquid scintillation counting using a Tri-Carb 2910TR analyzer (Perkin Elmer, Waltham, MA, USA). Lipogenic activity was normalized to total protein content per well.

Atherosclerosis quantification

Hearts from experiment 1 were formaldehyde fixated and paraffin embedded before cross-sectioning (5 μm) perpendicular to the axis of the aorta throughout the aortic root area. Sections were stained with hematoxylin-phloxine-saffron for histological analysis of lesion size and severity as described previously (*59*). Four subsequent sections per valve (50 μm distance) were analyzed starting from the first appearance of open aortic valve leaflets. Lesions were categorized by severity (mild, types I to III; severe, types IV and V) according to the guidelines of the American Heart Association adapted for mice (*26*). Quantification of macrophage content was performed using rat monoclonal anti-mouse MAC-3 antibody (1:1000; 550292; BD Pharmingen, San Diego, USA) and secondary goat anti-rat IgG (MP7444; Vector Laboratories Inc., Burlingame, USA). Cross sections were stained with monoclonal mouse antibody (1:1000; M0851; Dako, Heverlee, The Netherlands) against smooth muscle cell actin and secondary goat anti-mouse IgG (1:400; K4003; Dako,

Downloaded from https://www.science.org at Leiden University on March 06, 2026

Heverlee, The Netherlands) to quantify smooth muscle cell content. The immunoperoxidase complexes on the secondary antibodies were visualized with Nova Red (SK-4800, Vector Laboratories Inc., Burlingame, USA) and the Liquid Dab + Substrate Chromogen System (K3468, Dako, Heverlee, The Netherlands) for the macrophage and smooth muscle cell quantification, respectively. A solution of direct red and fast green (both 1:1000; 365548-5G and F7258S, respectively; Sigma-Aldrich, St. Louis MO, USA) was used to stain and quantify collagen. CCR2 was stained with a monoclonal rat Alexa Fluor 647 (AF647)–conjugated antibody (1:100; 150604; BioLegend, San Diego CA, USA), ICAM1 was stained with a primary monoclonal rat antibody (1:800; ab25375; Abcam, Cambridge, UK) and a secondary goat anti rat AF555-conjugated antibody (1:600; A214434, Invitrogen, Waltham MA, USA), VCAM1 was stained with a primary monoclonal rabbit antibody (1:250; ab134047; Abcam) and a secondary donkey anti rabbit AF647-conjugated antibody (1:600; A31573; Life Technologies, Carlsbad CA, USA), and CD3 was stained with a monoclonal rabbit antibody (1:100; ab16669; Abcam) and a secondary goat anti rabbit AF555-conjugated antibody (1:600; A21428; Invitrogen). For the fluorescent stainings, nuclei were stained with Hoechst 34580 (Thermo Fisher Scientific). Nonspecific fluorescence in the heart muscle did not affect the quantification within the lesion. Total lesion area and composition were assessed using ImageJ software (version 1.52a, National Institutes of Health, Bethesda, MD). Macrophage-, collagen-, and smooth muscle cell–positive lesion area was expressed relative to total lesion area of type III lesions. Lesion stability index of type III lesions was calculated as shown previously (*61*) per mouse by dividing the sum of relative collagen- and smooth muscle cell–positive lesion area by relative macrophage-positive area. Several mice from the IC7Fc and the combined treatment groups did not present type III lesions and were therefore excluded from this analysis, resulting in $n = 9$ to 16 for these lesion composition analyses. Similarly, a quantification of necrotic lesion cores found in type V lesions was not possible and is therefore not shown.

Flow cytometry

The following procedures were previously described in (*62*): Whole blood from experiment 1 collected after 7 weeks of treatment was incubated with hypotonic lysis buffer (160 mM ammonium chloride, 10 mM sodium bicarbonate, and 1.3 mM EDTA, pH 7.4) to remove erythrocytes. Samples were resuspended and stained in staining buffer (0.5% BSA and 5 mM EDTA in PBS, pH 7.4). Myeloid populations were identified using the following antibodies: αCCR2 (1:100, BV711, #747964, BD Biosciences, Franklin Lakes, NJ, USA), αCD11b (1:200, PerCP-Cy5.5, #550993, BD Biosciences), αCD11c (1:100, PE-Cy7, #25–0114, Thermo Fisher Scientific, Waltham, MA, USA), αCD16/32α (1:1000, #101330, BioLegend, San Diego, CA, USA), αCD45 (1:200, APC-Cy7, #103115, BioLegend), αLy6C (1:800, AF647, #128010, BioLegend), αLy6G (1:200, FITC, #11-5931, Thermo Fisher Scientific), αMHCII (1:200, BV510, #107635, BioLegend), and αSiglec-F (1:100, BV421, #562681, BD Biosciences). To identify T cell populations, samples were stained with the following antibodies: αCCR2 (1:100, BV711, #747964, BD Biosciences), αCD3 (1:200, APC-Cy7, #100306, BioLegend), αCD4 (1:400, BV421, 10443, BioLegend), αCD8 (1:1000, BV605, #100744, BioLegend), αCD16/32α (1:1000, #101330, BioLegend), αCD44 (1:200, FITC, #103006, BioLegend), αCD62L (1:1000, PE-Cy7, #104418, BioLegend), αCXCR3 (1:200, APC, #126511, BioLegend), and aCD25 (1:400, PE, 102008 BioLegend). Before analysis, 7AAD was added (final concentration of 10 μg/ml, A1310, Thermo Fisher Scientific) to exclude dead cells. Cells were measured on an LSR-Fortessa Cell Analyzer (BD Biosciences) and data were analyzed using FCS Express software, version 7 (De Novo Software). The following cell populations were defined: $CD4^+$ and $CD8^+$ naïve ($CD44^-$ $CD62L^+$), effector ($CD44^+$ $CD62L^-$), effector memory ($CD44^+$ $CD62L^{low}$), central memory ($CD44^+$ $CD62L^+$), C-C chemokine receptor type 2 $(CCR2)^+$ cells, regulatory T cells ($CD4^+$ $CD25^+$), nonclassical monocytes ($Ly6C^{low}$), and classical monocytes ($Ly6C^{hi}$). The gating strategy is shown in Supplementary Methods.

To analyze APOB quantity in the endogenously tagged HepG2-APOB-mNeon cells, the cells were detached, resuspended in fluorescence-activated cell sorting (FACS) buffer (PBS supplemented with 1% BSA and 5 mM EDTA), and measured on a CytoFLEX S Flow Cytometer (Beckman Coulter, CA, USA) using the 488-nm laser for excitation and the 525-nm fluorescent channel for emission. Acquired data were analyzed using FlowJo v10.8 Software (BD Life Sciences). Single live cells for analysis were gated using standard forward scatter versus side scatter gating.

Plasma measurements

Plasma TG and TC levels were measured using enzymatic Cobas Triglycerides (106571) and Cobas Total Cholesterol (106570) kits (both from Roche Diagnostics, Mannheim, Germany), by combining 7.5 μl of sample (5× diluted) with 200 μl of reagent before incubation at room temperature for 30 min and measuring absorption at 492 nm versus 650 nm (for TG) or at 505 nm versus 650 nm (for TC). Plasma HDL-c levels were quantified by precipitating APOB-containing lipoproteins from plasma by adding 20% polyethylene glycol in 200 mM glycine-buffered saline (pH 10), to subsequently measure TC in the supernatant as described above. Bile acid levels were measured in plasma collected at week 3 in experiment 3. Total bile acid levels were measured using a Total Bile Acids Assay (DZ042A, Diazyme, Dresden, Germany) according to the manufacturer's protocol.

Plasma IL-6, IL-10, TNF-α, and insulin concentrations were measured in freshly frozen plasma samples collected at week 7 in experiment 1 using a customized U-Plex Metabolic Group 1 (mouse) Kit (Meso Scale Discovery; Rockville, MD) or Ultra-Sensitive Mouse Insulin ELISA Kit (90080, Crystal Chem, Downers Grove, IL) according to the manufacturer's protocol.

Intestinal cholesterol absorption

Mice from experiment 1 were fasted for 4 hours before receiving a gavage of 1 μCi [^{14}C]cholesterol in 200 μl of olive oil. After 2 hours, mice were euthanized by CO_2 inhalation, perfused transcardially with ice-cold PBS for 5 min, and the content and tissue of duodenum, jejunum, and ileum as well as other peripheral tissues were collected and dissolved overnight at 55°C in 0.5 ml of Tissue Solubilizer (Amersham Biosciences, Rosendaal, The Netherlands). ^{14}C activity was determined in a Tri-Carb 2910TR Low Activity Liquid Scintillation Analyzer (Perkin Elmer, Waltham, MA) and expressed as percentage of the orally administered dosage.

Reverse cholesterol transport

In mice from experiment 1, in vivo reverse-cholesterol transport was determined as previously described (*63*). Female APOE*3-Leiden.CETP donor mice were intraperitoneally injected with 3%

Downloaded from https://www.science.org at Leiden University on March 06, 2026

Brewer's thioglycollate medium (Merck, Burlington, MA, USA) to induce the influx of macrophages into the peritoneum. After 4 days, donor mice received an intraperitoneal injection with 100 μg of acetylated LDL and 125 μCi [1,2-^{3}H(N)]cholesterol (Perkin Elmer, Waltham, MA, USA). After 1 hour, cholesterol-loaded peritoneal macrophages were isolated by peritoneal lavage with 10 ml of PBS. Macrophages were washed and resuspended in RPMI 1640 (ATCC, Manassas, VA, USA). Recipient mice received an intraperitoneal injection with 2×10^5 macrophages and were subsequently single housed for 72 hours during which feces were collected. Feces samples were freeze dried and dissolved overnight in Tissue Solubilizer (Amersham Biosciences, Roosendaal, The Netherlands) and 30% H_2O_2. ^{3}H activity was determined in a Tri-Carb 2910TR Low Activity Liquid Scintillation Analyzer (Perkin Elmer, Waltham, MA, USA), and expressed as percentage of the injected dose.

Fecal measurements

Fecal energy content was determined in experiment 1 as described before (*64*). Briefly, approximately 150 mg of dried and ground feces was burned in a Parr 6100 compensated calorimeter (Parr Instrument Company, Moline, IL, USA) using a 1108 Oxygen Bomb placed in 2000*g* of demineralized water. The increase in water temperature was used to assess fecal caloric content. Fecal neutral sterol content was measured as described previously (*65*). Briefly, approximately 50 mg of feces was incubated for 2 hours at 80°C in alkaline methanol, and neutral sterols were extracted three times with 3 ml of petroleum benzine. Neutral sterols were dried under nitrogen flow and derivatized by adding 100 μl of pyridine/N,O-bis(trimethylsilyl)trifluoroacetamide (BSTFA)/trimethylchlorosilane in a ratio of 50:50:1. The solution was incubated for 1 hour at room temperature and evaporated under nitrogen flow. Neutral sterols were solved in 1 ml of heptane with 1% BSTFA and concentrations were determined by gas chromatography (Agilent 6890, Amstelveen, The Netherlands) using a CPSil 19 capillary column (25 m by 0.25 mm by 0.2 μm) (Chrompack, Middelburg, The Netherlands) and 5α-cholestane as an internal standard (*66*).

Protein abundance

Frozen livers from experiment 1 were lyzed in PI3K buffer (1% Triton X-100, 10% glycerol, 137 mM NaCl, 2.7 mM KCl, 1 mM $MgCl_2$, 20 mM tris, pH 7.8, 10 mM NaF, 1 mM EDTA, 0.5 mM Na_3VO_4, 0.2 mM PMSF, and 1× protease and phosphatase inhibitor cocktail; Merck Millipore, Nottingham, UK) and homogenized with a FastPrep-24 5G Instrument (MP Biomedicals, Santa Ana, USA) using glass beads. The samples were placed on ice for 10 min and subjected to centrifugation (10 min at 12,000*g* at 4°C) before the supernatant was collected. HepG2 cells were lysed in RIPA buffer with protease and phosphatase inhibitors. Protein concentrations were determined using the Pierce BCA Protein Assay Kit (Thermo Fisher Scientific, Waltham, MA, USA). p-AMPKα^{Thr172}, AMPKα, p-ACC^{Ser79}, ACC, p-STAT3^{Tyr705}, and STAT3 were measured by using automated Western blot with Wes (ProteinSimple, Santa Clara, CA, USA), according to the manufacturer's protocol. Protein lysates were diluted to 0.8 μg/μl for all measurements except for the quantification of STAT3 for which the lysates were diluted to 0.2 μg/μl. The following antibodies from Cell Signaling (MA, USA) were used: phospho-AMPKα (Thr^{172}) (#2535, 1:50), AMPKα (23A3) (#2603, 1:50), phospho-acetyl-CoA carboxylase (Ser^{79}) (#3661, 1:20), acetyl-CoA carboxylase (#3662, 1:20), phospho-STAT3 (Tyr^{705}) (#9131, 1:50), and STAT3 (#9132, 1:20). GAPDH (#2118, Cell Signaling, 1:20) was used for normalization. For all antibodies, a secondary anti-rabbit antibody provided with the Wes kit (10 μl per well) was used. Compass software (ProteinSimple; v5.0.1) was used for analysis and quantification.

Gene expression analyses

RNA was isolated from frozen aortas and livers from experiment 1 by lysis and homogenization using TriPure RNA Isolation Reagent (11667165001, Sigma-Aldrich, St. Louis, USA) and a FastPrep-24 5G bead beating grinder and lysis system (4.0 m/s for 10 s; MP Biomedicals, Santa Ana, CA, USA). cDNA was subsequently synthesized from 1 μg of RNA using M-MLV Reverse Transcriptase (M1705, Promega, Madison, WI, USA) and quantitative polymerase chain reaction was performed using the SYBR green kit (Promega, Madison, Wisconsin, USA) and a CFX384 PCR machine (Bio-Rad, Hercules, CA, USA), according to the manufacturers' protocols. Gene expression was normalized to 60S acidic ribosomal protein P0 (*Rplp0*) and expressed relative to the Control group in experiment 1 and relative to the Chow control group in experiment 3. Primer sequences are provided in Table 1.

RNA from primary mouse hepatocytes was isolated using TriPure RNA Isolation Reagent and processed as above. Gene expression is shown relative to vehicle-treated control.

Hepatic VLDL production

After 3 weeks of treatment, mice from experiment 3 were fasted for 4 hours and anesthetized by intraperitoneal injection of ventranquil (6.25 mg/kg), midazolam (6.25 mg/kg), and fentanyl (0.31 mg/kg) in a total volume of 8 μl/g body weight, followed by subcutaneous injections of 50 μl every 45 min to sustain anesthesia. Subsequently, mice were injected intravenously with 10 μCi Tran[^{35}S] (MP Biomedicals, Eindhoven, The Netherlands) to label newly synthesized APOB. After 30 min, mice were injected intravenously with 10% Triton WR-1339 (5 μl/g body weight, Sigma-Aldrich, St. Louis, USA) to block LPL activity and thus VLDL-TG clearance. Blood was collected via the tail vein before and 15, 30, 60, and 90 min after the Triton WR 1339 injection, for measurement of plasma TG levels as described above. After 120 min, mice were exsanguinated via the retroorbital sinus. Plasma was ultracentrifuged in a density gradient, after which VLDL was isolated by aspiration (*67*). ^{35}S activity was measured in the acquired VLDL with and without the addition of 400 μl of isopropanol to precipitate APOB, and ^{35}S activity was expressed as DPM per milliliter, and VLDL-TG and VLDL-TC were measured as described above.

Hepatic cholesterol synthesis

Livers and plasma from mice supplemented with 5% deuterated water in experiment 3 were analyzed for cholesterol labeling. Frozen liver tissue (30 of 50 mg) was weighed and homogenized in 750 μl of PBS using an OMNI Bead Ruptor (OMNI International), and 5 μl of lysate was used for analysis. For blood plasma, 5 μl of a 1:10 dilution was used for analysis. The pipeline used for gas chromatography mass spectrometry lipid extraction first treats the sample with a mild acid methanolysis. Samples are incubated overnight at 45°C in a methanol/toluene/hydrochloric acid mixture, which is supplemented with 5-α-cholestane (Sigma-Aldrich C8003-100MG) as an internal standard. After incubation, lipids were extracted in 1 ml of hexane. A total of 25 μl was analyzed by gas chromatography mass

Downloaded from https://www.science.org at Leiden University on March 06, 2026

Table 1. Primer sequences.

Gene	Forward primer	Reverse primer
Abcb11	AAGCTACATCTGCCTTAGACACAGAA	CAATACAGGTCCGACCCTCTCT
Acaca	AACGTGCAATCCGATTTGTT	GAGCAGTTCTGGGAGTTTCG
Adgre1	CTTTGGCTATGGGCTTCCAGTC	GCAAGGAGGACAGAGTTTATCGTG
Apob	GCCCATTGTGGACAAGTTGATC	CCAGGACTTGGAGGTCTTGGA
Ccr2	TGCCATCATAAAGGAGCCA	AGCACATGTGGTGAATCCAA
Hmgcr	CCGGCAACAACAAGATCTGTG	ATGTACAGGATGGCGATGCA
Hnf4a	AGAAGATTGCCAACATCAC	GGTCATCCAGAAGGAGTT
Icam1	TCCGCTGTGCTTTGAGAACT	TCCGGAAACGAATACACGGT
Il1b	GCAACTGTTCCTGAACTCAACT	ATCTTTTGGGGTCCGTCAACT
Ly6c	CTGCAACCTTGTCTGAGAGGA	GTCCCTGAGCTCTTTCTGCAC
Mafg	GACCCCCAATAAAGGAAACAA	TCAACTCTCGCACCGACAT
Mcp1	AGCTGTAGTTTTTGTCACCAAGC	TGTCTGGACCCATTCCTTCTTC
Mttp	CTCTTGGCAGTGCTTTTTCTCT	GAGCTTGTATAGCCGCTCATT
Mvk	GCCTTGAACTTGAGAACTTTCC	CACCTGCTTAATACCGATGTTG
Nr0b2	CGATCCTCTTCAACCCAGATG	AGGGCTCCAAGACTTCACACA
Nr1h4	GGCCTCTGGGTACCACTACA	ACATCCCCATCTCTTTGCAC
Nr1h3	CTGCACGCCTACGTCTCCAT	AAGTACGGAGGCTCACCAGCT
Nr2f2	CCTCAAAGTGGGCATGAGAC	TGGGTAGGCTGGGTAGGAG
Pmvk	ACTTCGTGACCGAGAGGCTGAA	CTTGTAGGTGCTCGCATCCAGA
Rplp0	GGACCCGAGAAGACCTCCTT	GCACATCACTCAGAATTTCAATGG
Slc10a1	TGGCTACCTCCTCCCTGATG	GCCAGGTTGTGTAGGAGGAT
Slco1a1	TGAGAAAGACAGCAGTAGGACTTT	GTGATTTGGCTAGGTATGCAC
Slco1a4	TACATGTCAGCTTGCCTCGC	GCACACTCAGGACCCTTGTC
Slco1b2	GGGTGAATGCCCAAGAGACA	TATAGCCTGCATGCTCCACG
Srbebf1	AGCCGTGGTGAGAAGCGCAC	ACACCAGGTCCTTCAGTGATTTGCT
Tnfa	GCCTCTTCTCATTCCTGCTTG	CTGATGAGAGGGAGGCCATT
Vcam1	TGGAGGTCTACTCATTCCCTGA	GACAGGTCTCCCATGCACAA

spectrometry using an Agilent 7890B/5977B with DB-1HT column (Agilent 123-1131E). Cholesterol was quantified using a custom Python Tkinter software that analyzes sample data against a serial dilution of a separate cholesterol standard (Sigma-Aldrich C8667-1G). Detected ions from both samples and standards were integrated using the Mass Hunter Quantitative Analysis Program (Agilent Technologies). To measure newly synthesized hepatic cholesterol following deuterium treatment, enrichment of labeled cholesterol was quantified after correcting for naturally occurring stable isotopes using modern least squares implementation of the skewed matrix correction as we and others have published previously (*68*–*70*). Total cholesterol concentrations (in nanomoles per milligram) and percent labeled cholesterol were reported.

Liver analyses

Bile acids were extracted from the liver as described previously (*69*). Glyco-chenodeoxycholic acid (Sigma-Aldrich, G0759) and glycoursodeoxycholic acid (Sigma-Aldrich, 06863) were spiked into each sample as recovery standards at 5 nmol/μl. Bile acids were analyzed as described previously (*69*), with the following modification: the Ultimate3000 system was equipped with an ACE Excel C18-PFP UHPLC column (MAC-MOD Analytical, EXL10101502U).

To detect hepatic 7α-hydroxy-4-cholesten-3-one (C4), the column was replaced with an ACE Excel SuperC18 UHPLC Column (MAC-MOD Analytical, EXL10111502U). Buffer conditions were as follows: Mobile phase buffer A was 80% HPLC Water with 0.1% formic acid (Thermo Fisher Scientific): 20% Optima methanol and buffer C was 100% Optima methanol. Using a flow rate of 0.3 ml/min, a gradient method starting at 60% Buffer C increased to 90% by 2 min and then 100% by 5 min. Buffer C was held at 100% until 9 min then reduced to 60% by 10 min and maintained at 60% for 15 min. Equilibration for 0.5 min was performed using 60% Buffer C at the start of each sample run. The following parameters were used for sample ionization: polarity = positive; spray voltage = 3500 V; vaporizer temperature = 350°C; sheath and auxiliary gas (nitrogen) = 20 and 2 Arb resp.; ion transfer capillary temperature = 300°C; collision gas (argon) pressure = 1.5 mtorr; and collision energy = 10 to 25 V. Selected reaction monitoring was performed using the following: precursor mass/charge ratio (m/z) = 401.38; product 1 m/z = 383.33; product 2 m/z = 177.19; explicit collision energy (precursor, product) = 10, 25; and retention time = 7.5 min.

Liver bile acid extracts prepared for bile acid analysis were filtered, and 10 μl was injected into the liquid chromatography-mass spectrometry (LC-MS) via autoinjector. Five microliters each of serially

Downloaded from https://www.science.org at Leiden University on March 06, 2026

diluted C4 standards (Sigma-Aldrich 52853) was injected separately. C4 concentrations were quantified using Skyline-daily (MacCross Lab Software) from the C4 standard curve and exported with Molecule Setting set to MS level 2. The hepatic C4 was normalized to the percent recovery of the bile acid spike standards and then adjusted to total hepatic C4 by normalizing to total liver weight.

Liver tissue from experiment 3 was fixed first in 4% paraformaldehyde and subsequently in 30% sucrose before being embedded in optimal cutting temperature (OCT) embedding matrix (VWR, Radnor, PA, USA), frozen on dry ice, and sectioned (5 μm) before staining with hematoxylin and eosin and Oil Red O following standard protocols. The lipid-positive area was quantified using ImageJ software (version 1.53d, National Institutes of Health).

Liver tissue from experiment 1 was fixed in 4% paraformaldehyde overnight and dehydrated before paraffin embedding and sectioning (5 μm). Hematoxylin and eosin staining was performed following standard protocols. Histological evaluation of steatosis (severity 0 to 3) was conducted by a blinded reviewer.

Lipids were extracted from frozen liver tissue from experiment 1 using a modified version of the Bligh and Dyer protocol (*71*). Hepatic TG and TC content was measured as described above.

Statistical analyses

Significant outliers were identified with a Grubbs outlier test and removed from the analysis. Statistical analyses between groups were performed with unpaired *t* test or two-way ANOVA and following Tukey's or Šídák's multiple-comparison post hoc test, where applicable. Pearson's correlation coefficients were determined to assess linear correlations between variables. Linear regression analysis was used to calculate the slope of hepatic TG production in experiment 2. In experiment 3, the Chow control was used as healthy reference and not included in the statistical analyses. $P < 0.05$ was considered statistically significant. Statistical analyses were performed with GraphPad Prism software, version 9.3.1 (GraphPad, La Jolla, CA). Data are presented as individual data points and/or as means ± SD.

Supplementary Materials

This PDF file includes:

Supplementary Methods
Figs. S1 to S6

REFERENCES AND NOTES

1. G. A. Roth, G. A. Mensah, C. O. Johnson, G. Addolorato, E. Ammirati, L. M. Baddour, N. C. Barengo, A. Z. Beaton, E. J. Benjamin, C. P. Benziger, A. Bonny, M. Brauer, M. Brodmann, T. J. Cahill, J. Carapetis, A. L. Catapano, S. S. Chugh, L. T. Cooper, J. Coresh, M. Criqui, N. DeCleene, K. A. Eagle, S. Emmons-Bell, V. L. Feigin, J. Fernández-Solà, G. Fowkes, E. Gakidou, S. M. Grundy, F. J. He, G. Howard, F. Hu, L. Inker, G. Karthikeyan, N. Kassebaum, W. Koroshetz, C. Lavie, D. Lloyd-Jones, H. S. Lu, A. Mirijello, A. M. Temesgen, A. Mokdad, A. E. Moran, P. Muntner, J. Narula, B. Neal, M. Ntsekhe, G. Moraes de Oliveira, C. Otto, M. Owolabi, M. Pratt, S. Rajagopalan, M. Reitsma, A. L. P. Ribeiro, N. Rigotti, A. Rodgers, C. Sable, S. Shakil, K. Sliwa-Hahnle, B. Stark, J. Sundström, P. Timpel, I. M. Tleyjeh, M. Valgimigli, T. Vos, P. K. Whelton, M. Yacoub, L. Zuhlke, C. Murray, V. Fuster, GBD-NHLBI-JACC Global Burden of Cardiovascular Diseases Writing Group, Global burden of cardiovascular diseases and risk factors, 1990–2019: Update from the GBD 2019 study. *J. Am. Coll. Cardiol.* **76**, 2982–3021 (2020).
2. P. Libby, The changing landscape of atherosclerosis. *Nature* **592**, 524–533 (2021).
3. H. N. Ginsberg, C. J. Packard, M. J. Chapman, J. Borén, C. A. Aguilar-Salinas, M. Averna, B. A. Ference, D. Gaudet, R. A. Hegele, S. Kersten, Triglyceride-rich lipoproteins and their remnants: Metabolic insights, role in atherosclerotic cardiovascular disease, and emerging therapeutic strategies—A consensus statement from the European Atherosclerosis Society. *Eur. Heart J.* **42**, 4791–4806 (2021).
4. E. P. Navarese, D. Vine, S. Proctor, K. Grzelakowska, S. Berti, J. Kubica, P. Raggi, Independent causal effect of remnant cholesterol on atherosclerotic cardiovascular outcomes: A Mendelian randomization study. *Arterioscler. Thromb. Vasc. Biol.* **43**, e373–e380 (2023).
5. S. Rose-John, Interleukin-6 signalling in health and disease. *F1000Res* **9**, 1013 (2020).
6. P. M. Ridker, M. Rane, Interleukin-6 signaling and anti-interleukin-6 therapeutics in cardiovascular disease. *Circ. Res.* **128**, 1728–1746 (2021).
7. P. Van Der Harst, N. Verweij, Identification of 64 novel genetic loci provides an expanded view on the genetic architecture of coronary artery disease. *Circ. Res.* **122**, 433–443 (2018).
8. N. Sarwar, A. Butterworth, D. Freitag, J. Gregson, P. Willeit, D. Gorman, P. Gao, D. Saleheen, A. Rendon, C. Nelson, IL6R genetics consortium emerging risk factors collaboration. Interleukin-6 receptor pathways in coronary heart disease: A collaborative meta-analysis of 82 studies. *Lancet* **379**, 1205–1213 (2012).
9. D. Swerdlow, M. Holmes, K. Kuchenbaecker, J. Engmann, T. Shah, R. Sofat, Y. Guo, C. Chung, A. Peasey, R. Pfister, The interleukin-6 receptor as a target for prevention of coronary heart disease: A Mendelian randomisation analysis. *Lancet* **379**, 1214–1224 (2012).
10. M. Rosa, A. Chignon, Z. Li, M.-C. Boulanger, B. J. Arsenault, Y. Bossé, S. Thériault, P. Mathieu, A Mendelian randomization study of IL6 signaling in cardiovascular diseases, immune-related disorders and longevity. *NPJ Genom. Med.* **4**, 23 (2019).
11. P. M. Ridker, M. Devalaraja, F. M. Baeres, M. D. Engelmann, G. K. Hovingh, M. Ivkovic, L. Lo, D. Kling, P. Pergola, D. Raj, IL-6 inhibition with ziltivekimab in patients at high atherosclerotic risk (RESCUE): A double-blind, randomised, placebo-controlled, phase 2 trial. *Lancet* **397**, 2060–2069 (2021).
12. T. M. Kistner, B. K. Pedersen, D. E. Lieberman, Interleukin 6 as an energy allocator in muscle tissue. *Nat. Metab.* **4**, 170–179 (2022).
13. M. A. Febbraio, Role of interleukins in obesity: Implications for metabolic disease. *Trends Endocrinol. Metabol.* **25**, 312–319 (2014).
14. M. J. Kraakman, H. L. Kammoun, T. L. Allen, V. Deswaerte, D. C. Henstridge, E. Estevez, V. B. Matthews, B. Neill, D. A. White, A. J. Murphy, Blocking IL-6 trans-signaling prevents high-fat diet-induced adipose tissue macrophage recruitment but does not improve insulin resistance. *Cell Metab.* **21**, 403–416 (2015).
15. B. Rabe, A. Chalaris, U. May, G. H. Waetzig, D. Seegert, A. S. Williams, S. A. Jones, S. Rose-John, J. Scheller, Transgenic blockade of interleukin 6 transsignaling abrogates inflammation. *Blood* **111**, 1021–1028 (2008).
16. E. Boslem, S. Reibe, R. Carlessi, B. Smeuninx, S. Tegegne, C. L. Egan, E. McLennan, L. V. Terry, M. Nobis, A. Mu, Therapeutic blockade of ER stress and inflammation prevents NASH and progression to HCC. *Sci. Adv.* **9**, eadh0831 (2023).
17. S. Schreiber, K. Aden, J. P. Bernardes, C. Conrad, F. Tran, H. Höper, V. Volk, N. Mishra, J. I. Blase, S. Nikolaus, Therapeutic interleukin-6 trans-signaling inhibition by olamkicept (sgp130Fc) in patients with active inflammatory bowel disease. *Gastroenterology* **160**, 2354–2366.e11 (2021).
18. K.-J. Kallen, J. Grötzinger, E. Lelièvre, P. Vollmer, D. Aasland, C. Renné, J. Müllberg, K. H. Myer zum Büschenfelde, H. Gascan, S. Rose-John, Receptor recognition sites of cytokines are organized as exchangeable modules. Transfer of the leukemia inhibitory factor receptor-binding site from ciliary neurotrophic factor to interleukin-6. *J. Biol. Chem.* **274**, 11859–11867 (1999).
19. I. Gloaguen, P. Costa, A. Demartis, D. Lazzaro, A. Di Marco, R. Graziani, G. Paonessa, F. Chen, C. I. Rosenblum, L. H. Van der Ploeg, R. Cortese, G. Ciliberto, R. Laufer, Ciliary neurotrophic factor corrects obesity and diabetes associated with leptin deficiency and resistance. *Proc. Natl. Acad. Sci. U.S.A.* **94**, 6456–6461 (1997).
20. M. A. Febbraio, gp130 receptor ligands as potential therapeutic targets for obesity. *J. Clin. Invest.* **117**, 841–849 (2007).
21. D. Aasland, B. Schuster, J. Grotzinger, S. Rose-John, K. J. Kallen, Analysis of the leukemia inhibitory factor receptor functional domains by chimeric receptors and cytokines. *Biochemistry* **42**, 5244–5252 (2003).
22. M. Findeisen, T. L. Allen, D. C. Henstridge, H. Kammoun, A. E. Brandon, L. L. Baggio, K. I. Watt, M. Pal, L. Cron, E. Estevez, Treatment of type 2 diabetes with the designer cytokine IC7Fc. *Nature* **574**, 63–68 (2019).
23. M. Westerterp, C. C. van der Hoogt, W. de Haan, E. H. Offerman, G. M. Dallinga-Thie, J. W. Jukema, L. M. Havekes, P. C. N. Rensen, Cholesteryl ester transfer protein decreases high-density lipoprotein and severely aggravates atherosclerosis in APOE*3-Leiden mice. *Arterioscler. Thromb. Vasc. Biol.* **26**, 2552–2559 (2006).
24. M. G. Pouwer, E. J. Pieterman, N. Worms, N. Keijzer, J. W. Jukema, J. Gromada, V. Gusarova, H. M. Princen, Alirocumab, evinacumab, and atorvastatin triple therapy regresses plaque lesions and improves lesion composition in mice. *J. Lipid Res.* **61**, 365–375 (2020).
25. A. M. van den Hoek, J. W. A. van der Hoorn, A. Maas, R. van den Hoogen, A. van Nieuwkoop, S. Droog, E. Offerman, E. Pieterman, L. Havekes, H. Princen, APOE*3Leiden.CETP transgenic mice as model for pharmaceutical treatment of the metabolic syndrome. *Diabetes. Obes. Metab.* **16**, 537–544 (2014).

Downloaded from https://www.science.org at Leiden University on March 06, 2026

26. A. S. M. Zadelaar, L. S. Boesten, J. W. Jukema, B. J. van Vlijmen, T. Kooistra, J. J. Emeis, E. Lundholm, G. Camejo, L. M. Havekes, Dual PPARα/γ agonist tesaglitazar reduces atherosclerosis in insulin-resistant and hypercholesterolemic APOE*3Leiden mice. *Arterioscler. Thromb. Vasc. Biol.* **26**, 2560–2566 (2006).
27. B. Ason, J. W. van der Hoorn, J. Chan, E. Lee, E. J. Pieterman, K. K. Nguyen, M. Di, S. Shetterly, J. Tang, W.-C. Yeh, PCSK9 inhibition fails to alter hepatic LDLR, circulating cholesterol, and atherosclerosis in the absence of ApoE. *J. Lipid Res.* **55**, 2370–2379 (2014).
28. J. C. LaRosa, S. M. Grundy, D. D. Waters, C. Shear, P. Barter, J. C. Fruchart, A. M. Gotto, H. Greten, J. J. Kastelein, J. Shepherd, N. K. Wenger, Treating to New Targets (TNT) Investigators, Intensive lipid lowering with atorvastatin in patients with stable coronary disease. *N. Engl. J. Med.* **352**, 1425–1435 (2005).
29. S. J. Nicholls, C. M. Ballantyne, P. J. Barter, M. J. Chapman, R. M. Erbel, P. Libby, J. S. Raichlen, K. Uno, M. Borgman, K. Wolski, S. E. Nissen, Effect of two intensive statin regimens on progression of coronary disease. *N. Engl. J. Med.* **365**, 2078–2087 (2011).
30. I. Hilgendorf, F. K. Swirski, C. S. Robbins, Monocyte fate in atherosclerosis. *Arterioscler. Thromb. Vasc. Biol.* **35**, 272–279 (2015).
31. R. Saigusa, H. Winkels, K. Ley, T cell subsets and functions in atherosclerosis. *Nat. Rev. Cardiol.* **17**, 387–401 (2020).
32. X. Li, R. Liu, L. Zhang, Z. Jiang, The emerging role of AMP-activated protein kinase in cholestatic liver diseases. *Pharmacol. Res.* **125**, 105–113 (2017).
33. M. J. Watt, N. Dzamko, W. G. Thomas, S. Rose-John, M. Ernst, D. Carling, B. E. Kemp, M. A. Febbraio, G. R. Steinberg, CNTF reverses obesity-induced insulin resistance by activating skeletal muscle AMPK. *Nat. Med.* **12**, 541–548 (2006).
34. J. A. Ladias, M. Hadzopoulou-Cladaras, D. Kardassis, P. Cardot, J. Cheng, V. Zannis, C. Cladaras, Transcriptional regulation of human apolipoprotein genes ApoB, ApoCIII, and ApoAII by members of the steroid hormone receptor superfamily HNF-4, ARP-1, EAR-2, and EAR-3. *J. Biol. Chem.* **267**, 15849–15860 (1992).
35. A. Meurs, K. Ndoj, M. van den Berg, G. Marinkovic, M. Tantucci, T. Veenendaal, J. A. Kuivenhoven, J. Klumperman, N. Zelcer, A suite of genome-engineered hepatic cells provides novel insights into the spatiotemporal metabolism of apolipoprotein B and apolipoprotein B–containing lipoprotein secretion. *Cardiovasc. Res.* **120**, 1253–1264 (2024).
36. H. Ellingsgaard, E. Seelig, K. Timper, M. Coslovsky, L. Soederlund, M. P. Lyngbaek, N. J. Wewer Albrechtsen, A. Schmidt-Trucksäss, H. Hanssen, W. O. Frey, K. Karstoft, B. K. Pedersen, M. Böni-Schnetzler, M. Y. Donath, GLP-1 secretion is regulated by IL-6 signalling: A randomised, placebo-controlled study. *Diabetologia* **63**, 362–373 (2020).
37. R. van Eenige, Z. Ying, N. Tramper, V. Wiebing, Z. Siraj, J. F. de Boer, J. M. Lambooij, B. Guigas, H. Qu, T. Coskun, M. R. Boon, P. C. N. Rensen, S. Kooijman, Combined glucose-dependent insulinotropic polypeptide receptor and glucagon-like peptide-1 receptor agonism attenuates atherosclerosis severity in APOE*3-Leiden.CETP mice. *Atherosclerosis* **372**, 19–31 (2023).
38. P. P. Toth, Triglyceride-rich lipoproteins as a causal factor for cardiovascular disease. *Vasc. Health Risk Manag.* **12**, 171–183 (2016).
39. A. Riikola, K. Sipilä, M. Kähönen, A. Jula, M. S. Nieminen, L. Moilanen, Y. A. Kesäniemi, T. Lehtimäki, J. Hulkkonen, Interleukin-6 promoter polymorphism and cardiovascular risk factors: The Health 2000 Survey. *Atherosclerosis* **207**, 466–470 (2009).
40. J.-M. Fernández-Real, M. Broch, J. V. C. Richart, W. Ricart, Interleukin-6 gene polymorphism and lipid abnormalities in healthy subjects. *J. Clin. Endocrinol. Metabol.* **85**, 1334–1339 (2000).
41. A. S. Greenberg, R. P. Nordan, J. McIntosh, J. C. Calvo, R. O. Scow, D. Jablons, Interleukin 6 reduces lipoprotein lipase activity in adipose tissue of mice in vivo and in 3T3-L1 adipocytes: A possible role for interleukin 6 in cancer cachexia. *Cancer Res.* **52**, 4113–4116 (1992).
42. K. Nonogaki, G. M. Fuller, N. L. Fuentes, A. H. Moser, I. Staprans, C. Grunfeld, K. R. Feingold, Interleukin-6 stimulates hepatic triglyceride secretion in rats. *Endocrinology* **136**, 2143–2149 (1995).
43. A. L. Carey, G. R. Steinberg, S. L. Macaulay, W. G. Thomas, A. G. Holmes, G. Ramm, O. Prelovsek, C. Hohnen-Behrens, M. J. Watt, D. E. James, B. E. Kemp, B. K. Pedersen, M. A. Febbraio, Interleukin-6 increases insulin-stimulated glucose disposal in humans and glucose uptake and fatty acid oxidation in vitro via AMP-activated protein kinase. *Diabetes* **55**, 2688–2697 (2006).
44. F. W. Sanders, J. L. Griffin, De novo lipogenesis in the liver in health and disease: More than just a shunting yard for glucose. *Biol. Rev. Camb. Philos. Soc.* **91**, 452–468 (2016).
45. A. Di Pino, R. A. DeFronzo, Insulin resistance and atherosclerosis: Implications for insulin-sensitizing agents. *Endocr. Rev.* **40**, 1447–1467 (2019).
46. M. Hosel, M. Quasdorff, K. Wiegmann, D. Webb, U. Zedler, M. Broxtermann, R. Tedjokusumo, K. Esser, S. Arzberger, C. J. Kirschning, A. Langenkamp, C. Falk, H. Buning, S. Rose-John, U. Protzer, Not interferon, but interleukin-6 controls early gene expression in hepatitis B virus infection. *Hepatology* **50**, 1773–1782 (2009).
47. M. Le Vee, V. Lecureur, B. Stieger, O. Fardel, Regulation of drug transporter expression in human hepatocytes exposed to the proinflammatory cytokines tumor necrosis factor-α or interleukin-6. *Drug Metab. Dispos.* **37**, 685–693 (2009).
48. G. P. Hayhurst, Y. H. Lee, G. Lambert, J. M. Ward, F. J. Gonzalez, Hepatocyte nuclear factor 4alpha (nuclear receptor 2A1) is essential for maintenance of hepatic gene expression and lipid homeostasis. *Mol. Cell. Biol.* **21**, 1393–1403 (2001).
49. R. L. R. Abbing, D. Slijepcevic, J. M. Donkers, R. Havinga, S. Duijst, C. C. Paulusma, J. Kuiper, F. Kuipers, A. K. Groen, R. P. O. Elferink, Blocking sodium-taurocholate cotransporting polypeptide stimulates biliary cholesterol and phospholipid secretion in mice. *Hepatology* **71**, 247–258 (2020).
50. J. M. Donkers, R. L. R. Abbing, M. van Weeghel, J. H. Levels, A. Boelen, A. H. Schinkel, R. P. O. Elferink, S. F. van de Graaf, Inhibition of hepatic bile acid uptake by myrcludex B promotes glucagon-like peptide-1 release and reduces obesity. *Cell. Mol. Gastroenterol. Hepatol.* **10**, 451–466 (2020).
51. J. M. Donkers, S. Kooijman, D. Slijepcevic, R. F. Kunst, R. L. R. Abbing, L. Haazen, D. R. de Waart, J. H. Levels, K. Schoonjans, P. C. Rensen, R. P. O. Elferink, S. F. van de Graaf, NTCP deficiency in mice protects against obesity and hepatosteatosis. *JCI Insight* **5**, e127197 (2019).
52. X. Cheng, Y. Wang, J. Tian, L. Zhou, X. Chen, H. Guo, J. Zeng, N. Shen, J. Li, J. Ke, Y. Zhu, J. Gong, J. Chang, L. Liu, R. Zhong, SLC10A1 S267F variant influences susceptibility to HBV infection and reduces cholesterol level by impairing bile acid uptake. *J. Viral Hepat.* **26**, 1178–1185 (2019).
53. Y. Wada, C. Jensen, A. S. P. Meyer, A. A. M. Zonoozi, H. Honda, Efficacy and safety of interleukin-6 inhibition with ziltivekimab in patients at high risk of atherosclerotic events in Japan (RESCUE-2): A randomized, double-blind, placebo-controlled, phase 2 trial. *J. Cardiol.* **82**, 279–285 (2023).
54. S. Rose-John, The soluble interleukin 6 receptor: Advanced therapeutic options in inflammation. *Clin. Pharmacol. Ther.* **102**, 591–598 (2017).
55. B. Chen, S. Zhang, B. Wang, H. Chen, Y. Li, Q. Cao, J. Zhong, M. Xie, Z. Ran, T. Tang, DOP01 efficacy and safety of the IL-6 trans-signalling inhibitor olamkicept: A phase 2 randomized, placebo-controlled trial in moderately to severely active ulcerative colitis. *J. Crohn Colitis* **15**, S041–S042 (2021).
56. H. Schuett, R. Oestreich, G. H. Waetzig, W. Annema, M. Luchtefeld, A. Hillmer, U. Bavendiek, J. von Felden, D. Divchev, T. Kempf, K. C. Wollert, D. Seegert, S. Rose-John, U. J. F. Tietge, B. Schieffer, K. Grote, Transsignaling of interleukin-6 crucially contributes to atherosclerosis in mice. *Arterioscler. Thromb. Vasc. Biol.* **32**, 281–290 (2012).
57. D. M. Schulte, G. H. Waetzig, H. Schuett, M. Marx, B. Schulte, C. Garbers, J. Lokau, A.-K. Vlacil, J. Schulz, A. K. Seoudy, B. Schieffer, P. Rosenstiel, M. Seeger, M. Laudes, S. Rose-John, U. Lützen, K. Grote, S. Schreiber, Case report: Arterial wall inflammation in atherosclerotic cardiovascular disease is reduced by olamkicept (sgp130Fc). *Front. Pharmacol.* **13**, 758233 (2022).
58. B. Van Vlijmen, H. B. van't Hof, M. Mol, H. van der Boom, A. van der Zee, R. R. Frants, M. H. Hofker, L. M. Havekes, Modulation of very low density lipoprotein production and clearance contributes to age- and gender- dependent hyperlipoproteinemia in apolipoprotein E3-Leiden transgenic mice. *J. Clin. Invest.* **97**, 1184–1192 (1996).
59. M. J. Gijbels, M. van der Cammen, L. J. van der Laan, J. J. Emeis, L. M. Havekes, M. H. Hofker, G. Kraal, Progression and regression of atherosclerosis in APOE3-Leiden transgenic mice: An immunohistochemical study. *Atherosclerosis* **143**, 15–25 (1999).
60. E. H. Gilglioni, J. C. Chang, S. Duijst, S. Go, A. A. A. Adam, R. Hoekstra, A. J. Verhoeven, E. L. Ishii-Iwamoto, R. P. J. Oude Elferink, Improved oxygenation dramatically alters metabolism and gene expression in cultured primary mouse hepatocytes. *Hepatol. Commun.* **2**, 299–312 (2018).
61. C. Liu, M. Schonke, E. Zhou, Z. Li, S. Kooijman, M. R. Boon, M. Larsson, K. Wallenius, N. Dekker, L. Barlind, X. R. Peng, Y. Wang, P. C. N. Rensen, Pharmacological treatment with FGF21 strongly improves plasma cholesterol metabolism to reduce atherosclerosis. *Cardiovasc. Res.* **118**, 489–502 (2022).
62. B. Porteiro, R. L. P. R. Abbing, W. In Het Panhuis, D. R. de Waart, S. Duijst, I. Bolt, E. W. Vogels, J. H. M. Levels, L. A. Bosmans, W. G. Vos, R. P. J. O. Elferink, E. Lutgens, S. F. J. van de Graaf, Inhibition of hepatic bile salt uptake by Bulevirtide reduces atherosclerosis in Oatp1a1$^{-/-}$Ldlr$^{-/-}$ mice. *J. Lipid Res.* **65**, 100594 (2024).
63. Y. Zhang, I. Zanotti, M. P. Reilly, J. M. Glick, G. H. Rothblat, D. J. Rader, Overexpression of apolipoprotein AI promotes reverse transport of cholesterol from macrophages to feces in vivo. *Circulation* **108**, 661–663 (2003).
64. R. Li, A. Palmiotti, H. D. de Vries, M. V. Hovingh, M. Koehorst, N. L. Mulder, Y. Zhang, K. Kats, V. W. Bloks, J. Fu, H. J. Verkade, J. F. de Boer, F. Kuipers, Low production of 12α-hydroxylated bile acids prevents hepatic steatosis in Cyp2c70$^{-/-}$ mice by reducing fat absorption. *J. Lipid Res.* **62**, 100134 (2021).
65. J. F. de Boer, E. Verkade, N. L. Mulder, H. D. de Vries, N. Huijkman, M. Koehorst, T. Boer, J. C. Wolters, V. W. Bloks, B. van de Sluis, A human-like bile acid pool induced by deletion of hepatic Cyp2c70 modulates effects of FXR activation in mice. *J. Lipid Res.* **61**, 291–305 (2020).

Downloaded from https://www.science.org at Leiden University on March 06, 2026

66. C. Out, J. V. Patankar, M. Doktorova, M. Boesjes, T. Bos, S. de Boer, R. Havinga, H. Wolters, R. Boverhof, T. H. van Dijk, A. Smoczek, A. Bleich, V. Sachdev, D. Kratky, F. Kuipers, H. J. Verkade, A. K. Groen, Gut microbiota inhibit Asbt-dependent intestinal bile acid reabsorption via Gata4. *J. Hepatol.* **63**, 697–704 (2015).
67. T. Redgrave, D. Roberts, C. West, Separation of plasma lipoproteins by density-gradient ultracentrifugation. *Anal. Biochem.* **65**, 42–49 (1975).
68. J. P. Argus, A. K. Yu, E. S. Wang, K. J. Williams, S. J. Bensinger, An optimized method for measuring fatty acids and cholesterol in stable isotope-labeled cells. *J. Lipid Res.* **58**, 460–468 (2017).
69. B. L. Clifford, L. R. Sedgeman, K. J. Williams, P. Morand, A. Cheng, K. E. Jarrett, A. P. Chan, M. C. Brearley-Sholto, A. Wahlstrom, J. W. Ashby, W. Barshop, J. Wohlschlegel, A. C. Calkin, Y. Liu, A. Thorell, P. J. Meikle, B. G. Drew, J. J. Mack, H. U. Marschall, E. J. Tarling, P. A. Edwards, T. Q. de Aguiar Vallim, FXR activation protects against NAFLD via bile-acid-dependent reductions in lipid absorption. *Cell Metab.* **33**, 1671–1684.e4 (2021).
70. B. L. Parker, A. C. Calkin, M. M. Seldin, M. F. Keating, E. J. Tarling, P. Yang, S. C. Moody, Y. Liu, E. J. Zerenturk, E. J. Needham, M. L. Miller, B. L. Clifford, P. Morand, M. J. Watt, R. C. R. Meex, K. Y. Peng, R. Lee, K. Jayawardana, C. Pan, N. A. Mellett, J. M. Weir, R. Lazarus, A. J. Lusis, P. J. Meikle, D. E. James, T. Q. de Aguiar Vallim, B. G. Drew, An integrative systems genetic analysis of mammalian lipid metabolism. *Nature* **567**, 187–193 (2019).
71. E. G. Bligh, E. J. Dyer, A rapid method of total lipid extraction and purification. *Can. J. Biochem. Physiol.* **37**, 911–917 (1959).

Acknowledgments: We thank R. van Eenige, Z. Ying, M. Kamminga, R. Siebeler, L.A. Bosmans, and C.L. Egan for excellent technical support; E. Lutgens for providing the flow cytometry facility and antibodies; S.F.J. van de Graaf for providing the facility to measure plasma total bile acid levels; A.K. Groen for providing valuable input regarding data interpretation; and the National Biologics Facility (CSIRO Manufacturing, Clayton) for the production of IC7Fc. We would like to express our deepest gratitude to H.C.M. Sips who performed the protein analyses presented here but sadly passed away before the publication of this manuscript.
Funding: P.C.N.R. is supported by the Netherlands Cardiovascular Research Initiative: An initiative with support of the Dutch Heart Foundation (CVON-GENIUS-II). S.K. is supported by the Dutch Heart Foundation (2017T016). N.Z. is an Established Investigator of the Dutch Heart Foundation (2013T111) and is supported by a Vici grant from the Netherlands Organization for Scientific Research (NWO; 016.176.643) and an NWO ENW grant (M.22.034; GENESIS). S.Z. is supported by the Chinese Scholarship Council. M.R.d.V. is supported by a Rembrandt Institute for Cardiovascular Science grant. M.S. is supported by the Novo Nordisk Foundation (NNF18OC0032394). This work was supported by the Leiden University Fund (grant W213034-2-53 to M.S.). S.M.T.-N. is supported by the Australian Research Council (DP250102452). T.Q.d.A.V. is supported by National Institutes of Health (NIH) R01HL174008, R01HL163908, R01DK138340, and R01DK128952. M.A.F. is a Senior Principal Research Fellow of the NHMRC (APP1116936) and is also supported by an NHMRC Investigator Grant (APP1194141). Research in his laboratory was supported by project grants from the NHMRC (APP1042465, APP1041760, and APP1156511). **Competing interests:** M.A.F. is the founder and shareholder of Celesta Therapeutics and a consultant for Gallant Bio Pty Ltd. M.A.F. and S.R.-J. are the inventors of IC7 (patent number: 2008234408, patent title: "Treatment of obesity," filed by The Baker Heart & Diabetes Institute and granted by IP Australia in 2008). All other authors declare that they have no competing interests. **Author contributions:** Conceptualization: W.I.h.P., K.E.J., A.M., N.Z., J.F.d.B., M.A.F., P.C.N.R., and M.S. Methodology: K.E.J., A.M., M.R.d.V., S.R.-J., N.Z., T.Q.d.A.V., P.C.N.R., and M.S. Investigation: W.I.h.P., E.T., D.M.A.H.v.D., B.B., K.E.J., A.M., M.V.H., M.M., B.W.v.O., T.J.S., N.B., M.G., A.C.M.P., S.A., T.C.M.S., N.Z., M.O.T., S.Z., T.Q.d.A.V., L.V.T., and M.S. Formal analysis: W.I.h.P., B.W.v.O., D.M.A.H.v.D., K.E.J., T.C.M.S., B.B., M.O.T., N.Z., T.Q.d.A.V., and M.S. Visualization: W.I.h.P., N.Z., T.J.S., R.A.L., T.Q.d.A.V., and M.S. Data curation: M.R.d.V., K.E.J., M.O.T., T.J.S., T.Q.d.A.V., and M.S. Validation: K.E.J., M.R.d.V., L.V.T., T.Q.d.A.V., and M.S. Supervision: M.R.d.V., S.K., M.G., P.C.N.R., N.Z., T.Q.d.A.V., and M.S. Resources: T.E.A., S.M.T.-N., M.V.H., M.R.d.V., K.E.J., M.G., S.R.-J., N.Z., J.F.d.B., T.Q.d.A.V., M.A.F., and P.C.N.R. Funding acquisition: P.C.N.R., M.A.F., T.Q.d.A.V., and M.S. Project administration: P.C.N.R., T.Q.d.A.V., and M.S. Writing—original draft: W.I.h.P., M.A.F., and M.S. Writing—review and editing: All authors.
Data and materials availability: All data needed to evaluate the conclusions in the paper are present in the paper and/or the Supplementary Materials.

Submitted 11 March 2025
Accepted 24 September 2025
Published 24 October 2025
10.1126/sciadv.adx3794

Downloaded from https://www.science.org at Leiden University on March 06, 2026

Science Advances

The designer cytokine IC7Fc attenuates atherosclerosis development by targeting hyperlipidemia in mice

Wietse In het Panhuis, Ellen Thiemann, Daisy M. A. H. van Dijk, Bibian Been, Kelsey E. Jarrett, Amber Meurs, Sander Kooijman, Milaine V. Hovingh, Melanie Modder, Bram W. van Os, Thijs J. Sluiter, Niek Blomberg, Amanda C. M. Pronk, Salwa Afkir, Trea C. M. Streefland, Reshma A. Lalai, Maria O. Taveras, Sen Zhang, Timothy E. Adams, Lauren V. Terry, Sarah M. Turpin-Nolan, Margreet R. de Vries, Martin Giera, Stefan Rose-John, Noam Zelcer, Jan Freark de Boer, Thomas Q. de Aguiar Vallim, Mark A. Febbraio, Patrick C. N. Rensen, and Milena Schönke

Sci. Adv. **11** (43), eadx3794. DOI: 10.1126/sciadv.adx3794

View the article online
https://www.science.org/doi/10.1126/sciadv.adx3794
Permissions
https://www.science.org/help/reprints-and-permissions

Downloaded from https://www.science.org at Leiden University on March 06, 2026

Use of this article is subject to the Terms of service

Science Advances (ISSN 2375-2548) is published by the American Association for the Advancement of Science. 1200 New York Avenue NW, Washington, DC 20005. The title *Science Advances* is a registered trademark of AAAS.

Copyright © 2025 The Authors, some rights reserved; exclusive licensee American Association for the Advancement of Science. No claim to original U.S. Government Works. Distributed under a Creative Commons Attribution NonCommercial License 4.0 (CC BY-NC).